Michael Cheffena

Modeling and Prediction of Millimeter Wavelength Channels

Thesis for the degree of doctor philosophiae

Trondheim, August 2008

Norwegian University of
Science and Technology
Faculty of Information Technology, Mathematics and Electrical Engineering
Department of Electronics and Telecommunications

NTNU

Norwegian University of
Science and Technology

NTNU
Norwegian University of Science and Technology

Thesis for the degree of doctor philosophiae

Faculty of Information Technology, Mathematics and Electrical Engineering
Department of Electronics and Telecommunications

ISBN 978-82-471-1239-7 (printed ver.)
ISBN 978-82-471-1241-0 (electronic ver.)
ISSN 1503-8181

Theses at NTNU, 2008:271

Printed by Tapir Uttrykk

Modeling and Prediction of Millimeter Wavelength Channels

Michael Cheffena

DOCTORAL THESIS
FOR THE DEGREE OF PHILOSOPHIAE DOCTOR

Department of Electronics and Telecommunications
Norwegian University of Science and Technology

August, 2008

Abstract

The demand for high capacity data communication is increasing continuously and rapidly. More Network-based multimedia applications such as Internet protocol Television (IPTV), video on demand (VoD), voice over Internet protocol (VoIP), and other broadband services are emerging. Due to congestion in the lower frequency bands many of the services may use millimeter wavelength bands. A good understanding of the propagation impairments at millimeter wavelength is important for designing systems with a targeted quality-of-service (QoS) and availability.

Radio systems utilizing frequencies above about 10 GHz suffer from attenuation due to rain. Attenuation due to vegetation can severely degrade system performances as well. Estimation of the different time dynamic propagation impairments is essential for designing reliable and efficient communication systems. Depending on the current channel conditions such systems can adapt the transmission methodology to offer the required QoS and maximize the system throughput. The design of such mitigation technique requires knowledge of the different dynamic propagation impairments affecting the signal.

The research conducted in this study is on modeling and prediction of propagation effects at millimeter wavelength channels. The focus is on propagation effects between 20 - 60 GHz with emphasis on signal attenuation and fading due to rain and vegetation. The study has led to development of a new space-time rain attenuation model which can be used for simulating multiple correlated rain attenuation time series. Four years of measurement data from a star-like network was used in the analysis. Based on the spatial and temporal correlation of rain attenuation, a model for generating correlated multipath taps during rain for broadband fixed wireless access (BFWA) employed in dense urban area was developed. In addition, using available measurements the effect of rain on the performance of BFWA was investigated.

Duration statistics of rain attenuation are important when evaluating fade mitigation techniques (FMT) and estimating system outages. A study

on fade duration statistics for satellite links was performed using a large database compiled for this purpose. Based on this work, a new prediction model of fade duration statistics for satellite links operating between 10 - 50 GHz was developed.

The dynamic effects of vegetation were studied using available fading measurements at 2.45, 5.25, 29 and 60 GHz, and wind speed data. New models for simulating signal fading due to swaying vegetation were developed by using both a heuristic and theoretical approaches.

An initial dynamic wideband channel model for BFWA systems which combines degradations due to multipath propagation, rain and vegetation attenuation as well as scintillation effects was developed.

This work has contributed to and improved the ability to simulate propagation effects at millimeter wavelength channels. The models presented in this thesis can be used for simulating different capacity enhancing techniques such as adaptive coding and modulation and other FMT.

Preface

This dissertation is submitted in partial fulfillment of the requirements for the degree of *Philosophiae Doctor* (PhD) at the Department of Electronics and Telecommunications, Norwegian University of Science and Technology (NTNU). My main supervisor has been Associate Professor Torbjörn Ekman at the Department of Electronics and Telecommunications at NTNU, while my co-supervisor has been Dr. Lars Erling Bråten at the Norwegian Defence Research Establishment (FFI).

The studies have been carried out in the period from August 2005 to August 2008, including one semester of course work. Most of the time I worked at the University Graduate Center at Kjeller (UniK) outside Oslo, except from the period between April to December 2007, where I was a visiting researcher at the Communications Research Centre Canada (CRC) under the supervision of Dr. César Amaya.

The study was supported by the Research Council of Norway (NFR), via the project "Modeling and Prediction of Millimeter Wavelength Channels, Scheduling and Adaptive Data Rates for Wireless Access Systems (MoPSAR)" lead by Dr. Pål Orten currently working at ABB.

Acknowledgments

First and foremost I would like to thank my supervisors Lars Erling Bråten and Torbjörn Ekman for their valuable feedback, their positivism and guidance. They have been highly involved in the work leading to this thesis.

I am very grateful to my family and friends for supporting and encouraging me on this demanding project.

I am thankful to Telenor R&D for providing me with measurement data, especially I would like to thank Dr. Terje Tjelta for his ideas and valuable comments. I would also like to thank the Communications Research Centre Canada for their hospitality and for providing me further measurement data. I am especially grateful to Dr. César Amaya and Dr. Dave Rogers for

their useful comments and cooperation.

My thanks also goes to Ismail Hassan and David O. A. Ojelade for reviewing the introduction part of this thesis. Finally, I would like to thank all my fellow PhD students and researchers at Unik, especially Hans Jørgen Bang and Morten Pedersen for interesting discussions.

Oslo, August 2008
Michael Cheffena

Contents

Abbreviations

2G, 3G	Second to third generation of wireless (mobile) networks
ACF	Autocorrelation function
ACTS	Advanced communications technologies and services
AFD	Average fade duration
AGC	Automatic gain control
AOA	Angle of arrival
AOD	Angle of departure
AWGN	Additive white Gaussian noise
BER	Bit error rate
BFWA	Broadband fixed wireless access
BS	Base station
CDF	Cumulative distribution function
CCDF	Complementary cumulative distribution function
dB	Decibel
D-H	Dissanayake-Haidara
DSL	Digital subscriber line
ETSI	European telecommunications standards institute
FEC	Forward error correction
FMT	Fade mitigation techniques
GBSBE	Geometrical based single bounce elliptical
GPIB	General purpose interface bus
HPBW	Half power beamwidth
IPTV	Internet protocol Television
ITU	International telecommunication union
Km	Kilometer
LCR	Level crossing rate
LOS	Line-of-sight

MRC	Maximum ratio combiner
NFD	Non-fade duration
NLOS	Non-line-of-sight
OTS	Orbital test satellite
PDF	Probability density function
PMP	Point-to-multipoint
PNG	Papua new guinea
PSD	Power spectral density
QoS	Quality-of-service
RF	Radio frequency
RMS	Root mean square
RRM	Radio resource management
SEP	Symbol error probability
SINR	Signal-to-interference plus noise ratio
SIRIO	Satellite Italiano ricerca industriale orientata
SNR	Signal-to-noise ratio
TOA	Time of arrival
UT	User terminal
ULPC	Uplink power control
VoD	Video on demand
VoIP	Voice over Internet protocol
WiMAX	Worldwide interoperability for microwave access
WLAN	Wireless local area network

Part I

Introduction

Introduction

The increasing demands for high capacity data communications have required the use of higher frequencies. Services such as broadband communication, interactive broadcasting, multimedia applications and interconnection of local area networks require large bandwidths. Millimeter wavelength bands offer very large bandwidth compared to lower frequencies. Broadband fixed wireless access (BFWA) systems operating at millimeter wavelength are a means to provide everyone with true broadband services. They can offer cost efficient solutions and are an alternative to deploying cable based broadband access. BFWA can also function as a backbone for lower capacity systems such as wireless local area network (WLAN), worldwide interoperability for microwave access (WiMAX) and 2G - 3G base stations for mobile networks. To make such a BFWA system feasible, the initial cost for base stations (BSs) and user terminals (UTs) has to be low. The deployment of cheap hardware puts emphasis on the need for advanced signal processing to obtain reliable high data rate communication links. Moving the complexity from the hardware to the digital computations opens a wide range of research challenges.

A wireless system operating in the 20 - 45 GHz frequency bands is suitable for fixed and nomadic users. However, due to non-line-of-sight (NLOS) propagation in mobile channels these systems are not suitable for mobile users. The bandwidth will not be as scarce as for lower frequencies, but they are more sensitive to propagation degradation due to for example rain, scintillation and vegetation obstructions. A BFWA system will be quite similar to line-of-sight (LOS) radio links but it will differ in some important aspects:

- The BS will have to service a large number of UTs and will thus transmit over a sector instead of in a narrow beam. This might result in multipath even if the UTs have narrow beam antennas.
- In order to get good coverage we can not always require a free LOS path between the BS and UTs. There might be obstruction by vegetation or the dominant path might be a reflected one.

At millimeter wavelength a small change of pathlength can result in fast variations of the signal. It is sufficient that the antennas or any reflectors, as obstructing vegetation, sway in the wind a few millimeter to get fast fading channels. This combined with meteorological effects such as rain attenuation and scintillation will cause the channel to be time varying. The general approach in point-to-point radio links has been to apply fade mitigation techniques (FMT) or to add a large link margin to avoid the aforementioned effects. Focusing on low cost UTs the transmit power will be limited and the link margins smaller. In a multiuser system where the users have different channels the overall throughput can be improved by adjusting coding and modulation to the current channel conditions.

Rain attenuation varies slowly while scintillation and vegetation effects result in fast signal dynamics. The time duration of a fading event is crucial when it comes to what type of counter measures that should be applied. In general, the durations of fades due to rain events are longer compared to the one resulted from scintillation or vegetation effects. Short fades could be compensated for by interleaving and coding. Long fades which result in change of the average signal-to-noise ratio (SNR) can be compensated for by for example change of modulation and coding. Depending on how fast the channel varies, scheduling and data rate algorithms can be adapted to increase the system throughput and availability. Knowledge on the large but slow variations of the channel can be used to determine the average supported bit rate. This type of information can be signaled back to high layer applications to for example adjust the source coding for video or speech to the available data rates. Information on the short-term channel variations can for example be used to perform fast link adaptation. Figure 1.1 illustrates a point-to-multipoint (PMP) BFWA system affected by rain, vegetation and multipath. The signal could also be affected by combinations of different degradations for example rain and vegetation (both slow and fast fading), see the link with the dashed line in Fig 1.1. In this case, the fade counter measure should be optimized in terms of both the slow and fast fading dynamics that mitigate the effect simultaneously. Thus, understanding the dynamic propagation effects at millimeter wavelength channels are very important when designing FMT and evaluating system performance. This has therefore encouraged our research on *modeling and prediction of millimeter wavelength channels*.

The works are reported as collection of papers reproduced as part of this thesis. This introduction gives a background to the seven papers included in this thesis and a general overview of different propagation impairments at millimeter wavelength channels. In Section 1, different characteristics of rain attenuation are discussed. Sections 2 and 3 discuss the dynamic vege-

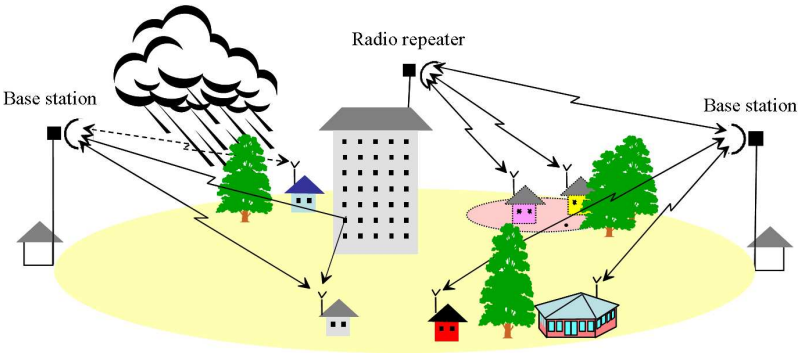

FIGURE 1.1: A point-to-multipoint BFWA system

tation effects and the multipath propagation in BFWA, respectively. A brief description of scintillation effects are given in Section 4. Discussions on the combined effects of different propagation degradations are dealt with in Section 5. Then, a description of the included papers is given in Section 6. Finally, Section 7 gives a conclusion by listing the main contributions of this thesis and presenting some suggestions for future research.

1 Rain Attenuation

At frequencies above 10 GHz, rain attenuation is often the main propagation impairment affecting a wireless communication system. The attenuation increases with increasing frequency [1]. Rain events occur almost randomly, especially convective rains affect communication systems for intervals comparable to the duration of popular services, such as TV and radio programs and Internet sessions. Figure 1.2 shows an example of a typical rain event measured from a 42 GHz terrestrial link at Rælingen, Norway which represents impairment due to rain and scintillation. The fast fluctuation with low amplitude corresponds to scintillation. The slowly varying component with large amplitude corresponds to rain attenuation. Rain affects radiowave propagation in three important ways [2]:

- The energy of the incident wave is absorbed by raindrops which are smaller than the wavelength through a basic heating effect. Depending on frequency, this will be the most significant source of rain attenuation.
- Larger raindrops on the order of wavelength in size will scatter the incident electromagnetic wave resulting in a reduction of the wave

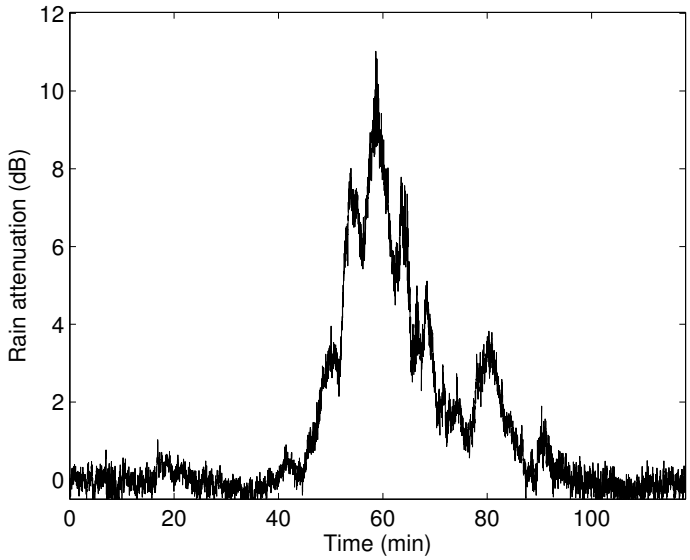

FIGURE 1.2: Measured rain attenuation at 42 GHz in Rælingen, Norway.

amplitude at the desired receiver location. The amount of scattering depends on the intensity of raindrops, size distribution and orientation.

- Raindrops cause depolarization of the incident wave, manly through scattering.

The attenuation on a radio path also depends on how much of the path that is subjected to rain. The specific rain attenuation in dB per km can be found though the following expression [3]

$$A = kR^{\alpha} \tag{1.1}$$

where k and α are constants which depend on frequency and polarization, and R is the rain rate in mm/h for a given percentage of time.

The international telecommunication union (ITU) [4] provides a global model for predicting the cumulative distribution function (CDF) of rain attenuation. The model gives the time percentage the attenuation exceeded in an average year and worst month. Figure 1.3 shows the complementary cumulative distribution (CCDF) of rain attenuation for a terrestrial link at Kjeller, Norway calculated using the ITU-R P.530 [4]. We can observe from Fig. 1.3 that high rain attenuation levels (greater than about 17 dB) can be observed for time percent less than 0.01% of an average year. Thus, em-

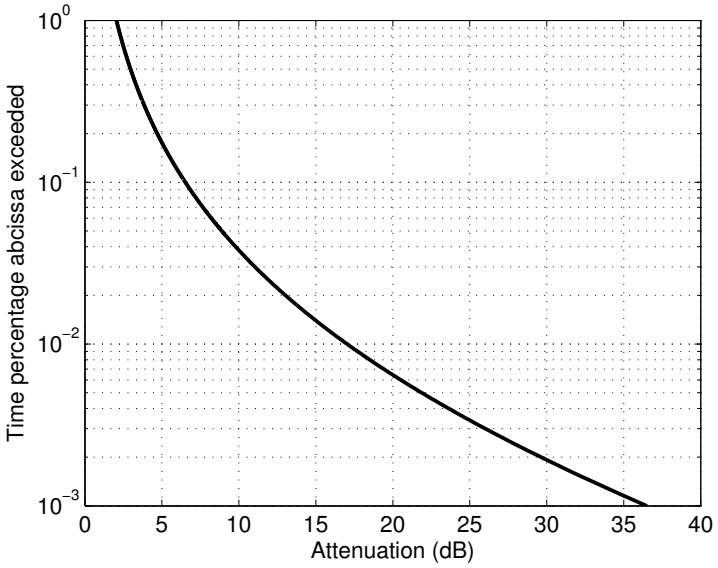

FIGURE 1.3: CCDF of rain attenuation for Kjeller 59.58^{o} N (latitude) and 11.02^{o} E (longitude) at 42 GHz and 4.6 km pathlength.

ploying a fixed fade margin may not guaranty the required quality of service at all times. Instead, FMT such as adaptive coding and modulation can be used to obtian the desired quality and availability to users. For example, during heavy rain conditions, power efficient modulation schemes can be used to prevent system outage. While spectral efficient modulation schemes can be used in clear sky conditions. Diversity techniques can be used during rain to increase system availability. The design and implementation of FMT requires knowledge of the first and second order statistics of rain attenuation. Second order statistics such as fade duration, inter-fade duration and fade slope describes the dynamic characteristics of rain attenuation, see Fig. 1.4.

In order to develop and test different FMT, data collected from propagation measurements are needed. Alternatively, time series generated from simulation models can be used. In this case, the simulated time series need to have similar statistical characteristics as those obtained from measurements.

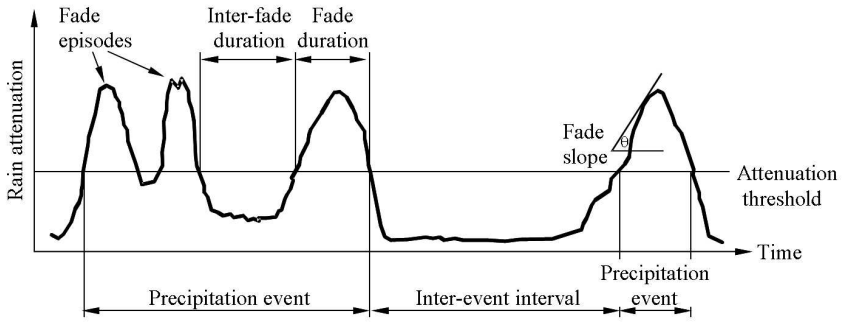

FIGURE 1.4: Dynamic features of rain attenuation [5]

1.1 Fade Duration

The duration of a fade is defined as the time interval between two consecutive crossings of the same attenuation threshold, see Fig. 1.4. The statistics can be described by two different CDFs [5]:

- $P(d > D|a > A)$, the probability of occurrence of fades of duration d longer than D (s), given that the attenuation a is greater than A (dB). This probability can be estimated from the ratio of the number of fades of duration longer than D to the total number of fades observed, given that the threshold A is exceeded.
- $F(d > D|a > A)$, the cumulative exceedance probability, or, equivalently, the total fraction (between 0 and 1) of fade time due to fades of duration d longer than D (s), given that the attenuation a is greater than A (dB). This probability can be estimated from the ratio of the total fading time due to fades of duration longer than D given that the threshold A is exceeded, to the total exceedance time of the threshold.

Fade duration is an important parameter to be taken into account in system design for several reasons:

- *System outage and unavailability*: Fade duration statistics provides information on the number of outages and the probability of the system being unavailable for a time period of a given duration.
- *Fade mitigation techniques*: Depending on the link margin, fade duration statistic provides statistical information on the time durations the system stays in a compensation configuration.
- *Coding and modulation*: Fade duration is a key element in the process

of choosing forward error correction codes and best modulation schemes. The propagation channel does not produce independent errors but blocks of errors. Fade duration impacts directly on the choice of the coding scheme.

Fade duration distributions of rain attenuation are often modeled as the sum of two functions, one taking account of short durations and the second accounting for long durations [5–8]. The short and long durations are usually assumed to be caused by scintillation and rain effects, respectively. There also exist models which uses three functions to describe the fade durations due to scintillation, convective and stratiform rains [9].

1.2 Inter-Fade Duration

The inter-fade duration or non-fade duration (NFD) is the complement of the fade duration, see Fig. 1.4. In addition to the fade duration, it is also important to characterize the time interval between two fades. Once the level of the received signal has just crossed back over the margin threshold after an outage event, it is essential to know statistically the duration before the occurrence of another fade event which may result in system outage. The inter-fade duration can be classified in to short, intermediate and inter-event intervals [10]. The short inter-fade interval segment accounts for tropospheric scintillation, and any fast amplitude variations resulting from rapid changes in rain dynamics. This interval ranges approximately from 1 to 10 seconds. The intermediate range results from rain dynamics such as rain cell translation, and life cycle variations of rain cells. The range of the intermediate interval is approximately from 10 seconds to several hours. The inter-event intervals are measured in days and represent the distribution of return periods of rain events [10]. Several studies and experimental results of inter-fade duration of rain attenuation are reported in the literature, among them are [10–14].

1.3 Fade Slope

Fade slope describes the rate of change of rain attenuation, see Fig. 1.4. A typical fade countermeasure system is open-loop uplink power control (ULPC), in which the attenuation on a uplink is estimated from the attenuation measured on the downlink and compensated by varying uplink power [15]. Information regarding on fade slope is therefore important for determining the required tracking speed of the ULPC. Fade slope depends on the attenuation level and the rain rate [16, 17]. This implies that the fade slope will depend on the drop size distribution and therefore on the type

of rain (convective or stratiform rain) [18]. Another parameter of influence is the horizontal wind velocity perpendicular to the path which determines the speed at which the horizontal rain profile passes across the propagation path. The fade slope is likely to decrease with increasing pathlength. This is because a certain attenuation level on a longer path is more likely to be caused by widespread rain, or by several rain cells integrated over a longer distance, while the same attenuation on a shorter path is more likely to be due to a single, more intense rain cell [18]. Several prediction models of fade slope distribution has been published in the literature, among them are [18–22].

1.4 Temporal and Spatial Variability of Rain Attenuation

Rain attenuation shows a temporal and spatial variability. Depending on the temporal and spatial correlation of rain attenuation different paths may experience correlated attenuations. It is often observed that during showers, high intensity rain is localized in a small area surrounded by a region of more uniform, low intensity rain [1]. The spatial and temporal rain attenuation correlation shows a seasonal dependency, were the correlation is smaller during summer than during winter. This is because relatively small rain cells with high rainfall rates (convective rain) occur more frequent during summer than during winter. Similarly, stratified rainfall, which extends over larger areas with small rainfall rates, occur more frequent during winter than during summer [23, 24]. Fig. 1.5 illustrates a link diversity configuration during rain where a UT is simultaneously connected to two BSs at any time. In this scenario, information on space-time correlation of rain attenuation can be used by the system to select the most suitable base station for the user. In a millimeter wavelength PMP systems, high capacity can be gained by using a combination of coding and diversity [25]. To obtain this, knowledge of the spatial and temporal variation of rain attenuation is needed. This channel information is also useful for adaptive data rate algorithms. Depending on the spatial and temporal variation of rain attenuation the overall system performance can be improved by adapting the modulation and coding to the current channel conditions.

A number of models describing the temporal variability of rain attenuation can be found in the literature, among them [26–32], and models describing the horizontal distribution of rain attenuation [33, 34]. It is of great interest to have a space-time rain attenuation model which combines the temporal and spatial variability of rain attenuation. Depending on the separation angle between different links and climatic parameters, such a model can be used for generating multiple correlated rain attenuation time

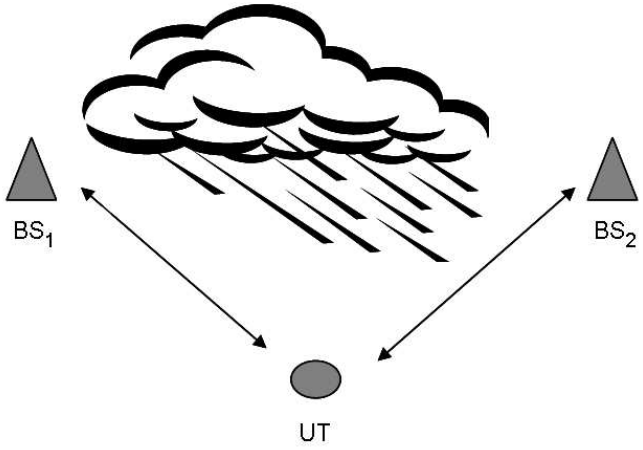

FIGURE 1.5: Route diversity during rain, where a user terminal selects a link from base station with a lower attenuation at any time.

series experienced by each link. This can further be used for optimizing FMT such as link diversity, space-time coding and other performance enhancing techniques.

2 Vegetation Effects

Vegetation obstructing the LOS propagation path causes radiowave absorption, scattering, diffraction and depolarisation [35]. The attenuation depends on a range of factors; among them are tree type, whether trees are in leaf or without leaf, whether trees are dry or wet, frequency, and path-length through foliage [36, 37]. The ITU-R P. 833 [38] provides a model for predicting the mean signal attenuation though vegetation. At millimeter wavelength leaves and needles have dimension large compared to the wavelength, and can significantly affect the propagation condition. For a receiver sight obstructed by vegetation, the channel does not remain static as vegetation move due to applied wind force. In some cases, the signal can be insufficient for service after propagating through vegetation. In other cases, a UT may be obstructed by vegetation along the signal path that does not give a sufficient mean attenuation to take the received signal level below the system margin. However, as the trees move with wind, time varying multipath component occur due to reflection and scattering from swaying tree components. This results in signal level variation over a large range which may make the provision of a service unfeasible. Fig. 1.6 shows an example of a typical measured received signal at 29 GHz after

propagating through a leaved dry deciduous trees and the corresponding measured wind speed is shown in Fig. 1.7. As expected the signal variation increases with increasing wind speed. Observe the large signal variations in Fig. 1.6 after about 2000 seconds which is caused by the increase in wind speed shown in Fig 1.7. This indicates the existence of high correlation between received signal variation through vegetation and wind speed. In general, designing mitigation techniques for these very fast and deep signal variations can be challenging and it depends on accurate modeling and prediction of the signal fading. This further requires the knowledge of wind dynamics and the complex response of a tree to induced wind force. Different experimental results and analysis on the effect of vegetation on radiowaves are reported in the literature; among them are [36, 37, 39–44].

Much research in the past has been concentrated in characterizing the mean attenuation through vegetation. Understanding the dynamic effects are essential, especially having time series synthesizers for signal fading due to swaying vegetation are important for testing different system implications due to vegetation. In this case, the simulation model should have similar statistical and dynamical characteristics as those of measurements. Time series obtained from propagation experiments can be used for this purpose. However, such time series may not be available at the preferred frequency, wind speed conditions etc.

3 Multipath Propagation

Multipath propagation occur when the received signal consists of a number of signals that have traveled different pathlengths. Multipath propagation with large time delays relative to symbol duration result in frequency selective fading, which can significantly degrade the system performance if no equalizers are used. The time delay between received multipath components depend on both the surrounding reflectors and the properties of the transmitting and receiving antennas. A ray-tracing study reported in [39] shows that the very narrow user terminal antenna beamwidths in BFWA systems cause the majority of multipath signals to be heavily attenuated. Only the very shallow grazing rays from nearby rooftops and the ground enter the receiver with an appreciable magnitude. Fig. 1.8 shows a possible multipath scenario at millimeter wavelength signal in urban environment. In addition to the desired LOS signal, reflections from nearby building of the desired transmitted signal (and also of undesired interfering signals) may occur. In the millimeter wavelength region the diffraction phenomenon can be neglected and the sum of the direct ray and the re-

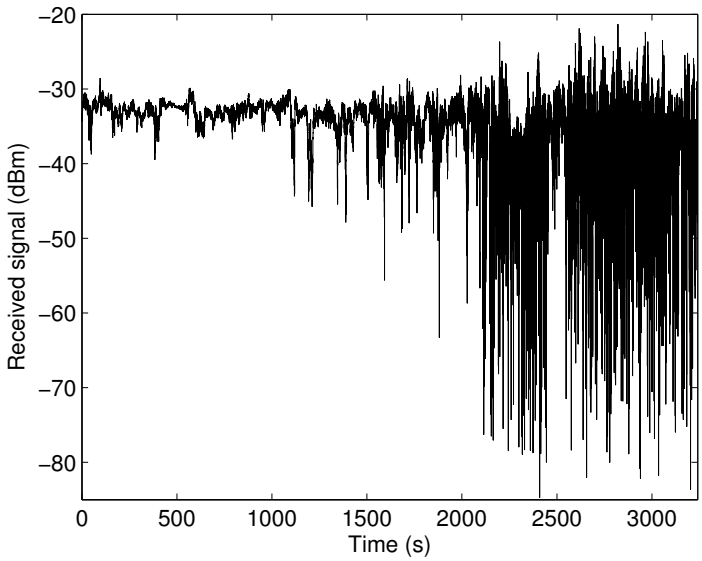

FIGURE 1.6: Measured signal fading after propagating through dry leaved deciduous trees at 29 GHz.

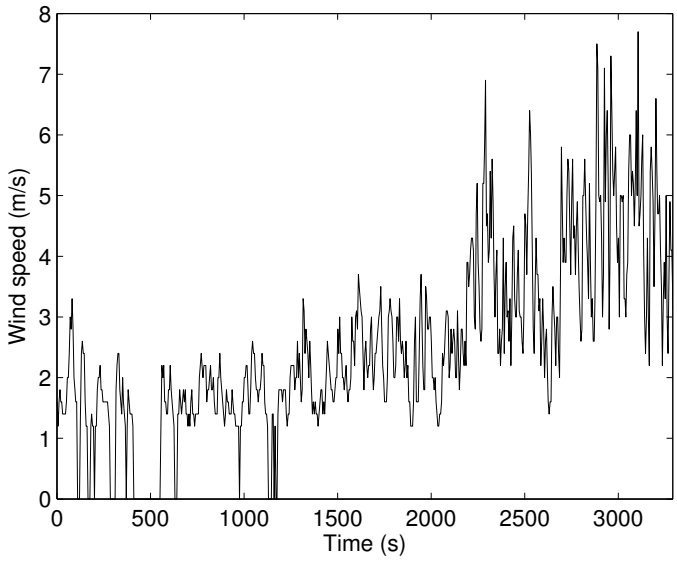

FIGURE 1.7: Measured wind speed.

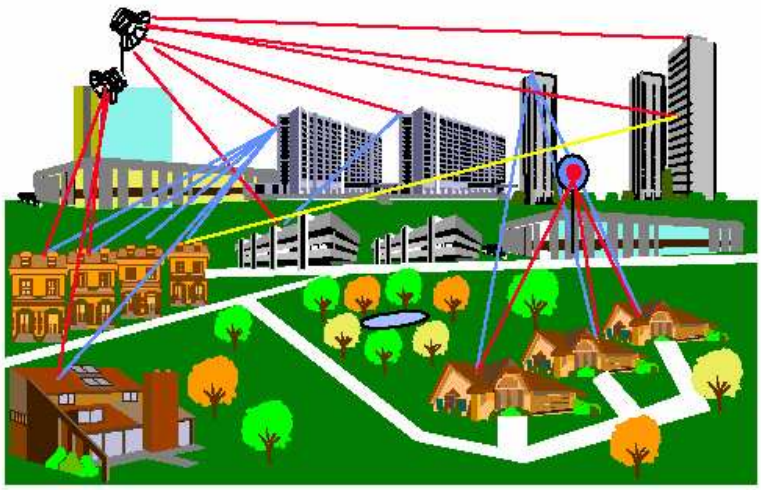

FIGURE 1.8: Multipath in BFWA system (at millimeter wavelength) employed in urban environment [39].

flected/scattered rays can be used to describe the behavior of the propagation channel with good accuracy [45, 46]. Building surfaces are quite rough at millimeter wavelength, and this leads to diffuse reflection [47].

The distribution of the short-term received signal envelope after propagating different paths can be described by a Nakagami-Rice distribution [48, 49]. The change of the reflection properties in the environment due to wet surfaces can cause time varying multipath propagation [49]. It was found from 38 GHz wideband measurements that the Nakagami-Rice K-factor of the received signal decreases with increasing rain rate, and is given by [49]

$$K = 16.88 - 0.04R \tag{1.2}$$

where R is the rain rate in mm/h. This is because wet surfaces become better reflectors which results in increasing specular reflected power. In order to characterize the multipath property of a given environment, the location of each reflector has to be known. Ray tracing techniques using geographical databases may obtain reflector locations, however in many cases these databases are not available. More generic representation of the propagation channel can be obtained by getting the location of reflectors from a statistical distribution. In recent years a number of experimental results and multipath models for BFWA has been reported, among them are [48–53].

4 Scintillation Effects

The random variations of the refractive index caused by atmospheric turbulence yields a random variation of the amplitude, phase and angle of arrival (AOA) of the received signal. This phenomenon is called tropospheric scintillation. In the troposphere, there are two main regions in which turbulence is likely to be strong. In the lower part of the troposphere (the surface boundary layer) where turbulence fluctuations produce mixing of the air, and are responsible for vertical transport processes near the Earth's surface. In clouds, where turbulence results from the entrainment of air (the process by which the outer edge of the cloud mixes with dry air outside of the cloud) [39]. It has been shown that turbulence in cumulus clouds (especially fair-weather clouds) induces most of the scintillation effects observed on satellite links [39]. The scintillation effects observed on terrestrial links are mainly due to turbulence in the lower part of the atmosphere [54]. The amplitude of scintillations increases with increasing frequency, pathlength, and antenna beamwidth [55–57]. In addition to clear sky scintillation, scintillation occurs also simultaneously during rain induced fades where the standard deviation of scintillation increases with increasing rain attenuation [58].

A wide aperture antenna may be used to reduce the effect of scintillation, since this produces averaging of the scintillation across the slightly different paths taken to each point across the aperture. Alternatively, spatial diversity may be used, where the signals from two antennas are combined to reduce the overall fade depth (best result may be obtained by using vertically separated antennas due to the tendency for horizontal stratification of the troposphere [59]). Numerous studies dealing with scintillation can be found in the literature, among them are [54–64].

5 Combined Propagation Effects

In some cases the received signal can be affected by combinations of different propagation degradations [65, 66]. For example the received signal may be affected by rain, scintillation, vegetation and multipath propagation. In order to design and optimize a FMT for such scenario, knowledge of the individual propagation effects and their dependency on each other is required. As discussed in Section 4, during rain the scintillation standard deviation increases with increasing rain attenuation [58]. In Section 3 the dependency of the received multipath signal power on rain rate was discussed, where the Nakagami-Rice K-factor decreases with increas-

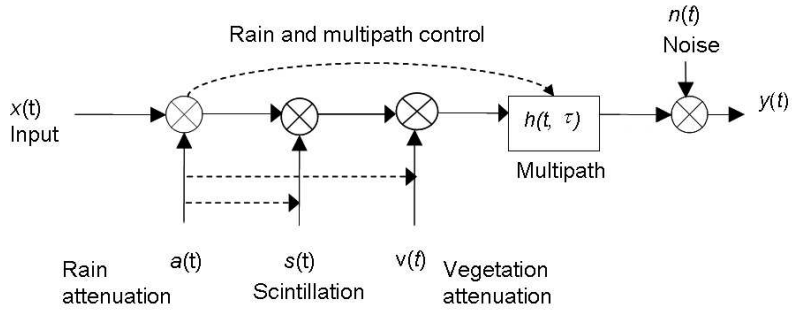

FIGURE 1.9: Combined wideband dynamic channel model [65, 66].

ing rain rate due to increase power of the reflected multipath components [49]. Measurement results in [37] shows that wet vegetation attenuates the signal more than dry ones. Fig. 1.9 illustrates a channel model for combined propagation effects. The dashed lines indicate that there is a dependency between the propagation effects. The channel impulse response is then given by

$$h(t) = \sum_{n=0}^{N-1} a_n(t)s_n(t)v_n(t)m_n(t)\delta(t-\tau_n)\exp(-j\phi_n(t)) \tag{1.3}$$

where t is the time and N is the total number of taps. For each tap number n, $\tau_n(t)$ is the tap delay, $\phi_n(t)$ is the phase within the range [0, 2π], δ is delta function, $m_n(t)$ is the signal amplitude, $v_n(t)$ is the time varying vegetation attenuation, $s_n(t)$ is the scintillation effect and $a_n(t)$ is the dynamic rain attenuation. Depending on the pathlength traveled through vegetation, rain and turbulence, each tap will have different average vegetation and rain attenuations, and scintillation effects. Foliage density is not uniform, which implies that depending on the angle of incident to the foliage, taps will fade differently. During rain, the taps may be subjected to varying correlated dynamics depending on the spatial correlation of rain attenuation between different paths though rain [66]. In general, understanding the different dynamic propagation effects at millimeter wavelength and their dependency on each other is important for developing a realistic wideband combined channel model. The model can be used for simulating FMT for combinations of different propagation impairments.

6 Contributions of the Included Papers

This thesis incorporates seven papers. Propagation impairments due to rain, vegetation and multipath propagation were investigated. Paper A focuses on rain attenuation, and investigates the spatial and temporal variability of rain attenuation. Based on the model and theory on the spatial and temporal correlation of rain attenuation described in Paper A, the multipath propagation during rain in BFWA employed in dense urban areas was studied in Paper B. The objective was to develop a theoretical model for simulating correlated channel tap realizations during rain which can be used in performing different system aspect simulations.

In Paper C we concentrated on satellite links and studied the fade duration statistics for frequencies between 10 - 50 GHz, and proposed a new prediction model. While in Paper D the focus was to investigate the effect of rain attenuation on the channel capacity and bit error rate (BER) of BFWA systems.

Papers E and F deals with the dynamic effects of vegetation on propagating radiowaves, and new models for simulating signal fading due to swaying vegetation were developed. Finally, Paper G presents a wideband dynamic channel model which combines propagation impairments due to rain, scintillation, vegetation and multipath propagation.

Please note that the models for the multipath and vegetation effects presented in Paper G can be replaced by the models developed in Paper B and E/F, respectively. A brief summary of the individual papers is given below.

Paper A

Michael Cheffena, Lars Erling Bråten, and Torbjörn Ekman, "Dynamic Space-Time Rain Attenuation Model," Submitted August 2007, Revised June 2008 to *IEEE Transactions on Antennas and Propagation.*

This paper is partially based on a previously published conference article [67]. We have investigated the space-time correlation of rain attenuation using 42 GHz star-like network measurements. By combining the spatial and temporal variability of rain attenuation we developed a new model for synthesizing multiple correlated rain attenuation time series. The model is based on the Maseng-Bakken model reported in [26]. Many of reported time series synthesizers of rain attenuation are focused on generating time series of one link. However, giving the degree of rain attenuation correla-

tion between two or more links, the model can be used to generate multiple correlated rain attenuation time series which can be used for optimizing FMT and for simulating capacity enhancing techniques such as route diversity, space-time coding and adaptive coding and modulation. The correlation properties of the model were validated by comparing it with published diversity gain models. Good agreement was also found between measured and simulated CDFs of rain attenuation. The model parameters were extracted from available measurements at 42 GHz.

In the Maseng-Bakken model the dynamics of rain attenuation is controlled by the parameter β_s. Using β_s values extracted from our measurements and other previously reported values in the literature, we identified the most significant climatic and link parameters which influences the rain attenuation dynamics. From this we constructed a prediction model for β_s using systematic multivariable technique reported in [68]. Finally, we studied the advantage of route diversity with selection combing using available measurements.

Paper B

Michael Cheffena and Torbjörn Ekman, "Theoretical Multipath Channel Model During Rain for BFWA Employed in Dense Urban Areas," Accepted for publication in *Proc. 2nd International Conference on Signal Processing and Communication Systems*, Gold Coast, 15 - 17 December, 2008.

During rainfall, the multipath taps may be subjected to varying correlated dynamics depending on the spatial correlation of rain attenuation between different paths though rain. Based on the theory described in Paper A on the spatial and temporal correlation of rain attenuation, a theoretical model for generating correlated multipath taps during rain for BFWA employed in dense urban area was developed. Using the developed theoretical model, we investigated the role of UT antenna on the performance of BFWA. The results show that system outage increases with increasing antenna beamwidth. Especially, a rapid variation of the outage probability was observed for antenna beamwidth between 1 - 5 degree. The results indicate the importance of narrow beam UT antennas in BFWA systems. The model can be used for performing other different system level analysis.

Paper C

Michael Cheffena and César Amaya, "Prediction Model of Fade Duration Statistics for Satellite Links between 10 - 50 GHz," Accepted for publication in *IEEE Antennas and Wireless Propagation Letters*, to appear in 2008.

In paper C we developed a new model for predicting fade duration statistics for satellite links between 10 - 50 GHz using statistics derived from unfiltered beacon data. A large fade duration database which covers the Ku, Ka, and Q/V frequency bands, different elevation angles (14^o - 89^o) and a variety of different climatic conditions (tropical, sub-tropical and temperate) was used. Two lognormal functions were used to model the short and long durations due to scintillation and rain events. The individual variables in the double lognormal are modeled as functions of link and climatic parameters. A systematic multivariable technique reported in [68] was used to identify the most significant parameters that governs the fade duration statistic of a given location. The parameters found are the attenuation threshold, frequency, elevation angle and the Rice-Holmberg [69] rain convectivity parameter. Then, we compared the performance of the new model with well known existing prediction models such as the ITU-R [5], COST 205 [6] and Dissanayake-Haidara (D-H) [7]. The results show that the new model has the best performance at Ku, Ka, and Q/V frequency bands. When comparisons were performed using all available data, the new model gives the best prediction on average, followed by the D-H, COST 205 and the ITU-R models, respectively.

Paper D

Michael Cheffena, "The Effect of Rain Attenuation on the Performance of BFWA around Kjeller, Norway," Accepted for publication in *Proc. IEEE 68th Vehicular Technology Conference* (*VTC*), Calgary, 21 - 24 September, 2008.

Paper D treats the transmission issues in a combined form including both propagation effects and system aspects. The effect of rain attenuation on the performance of BFWA around Kjeller, Norway was investigated using rain attenuation statistics derived from local measurements at 42 GHz collected over four years from a star-like network. The rain attenuation statistics of three converging links is presented and compared with the ITU-R model [4]. The results show that the ITU-R model predicts the statistics relatively well, expect for high attenuation levels where the model overestimates the occurrence. During rain, the stochastic nature of

the propagation channel is transferred to the channel capacity and BER statistics. Statistical results of the channel capacity and BER in the presence of rain attenuation at different service distances in scenarios with and without intercell interference are presented. The results give an insight to the effect of rain attenuation on system performance, and can be used for evaluating the technical feasibility of BFWA systems in locations with weather conditions similar to the Kjeller area.

Paper E

Michael Cheffena and Torbjörn Ekman, "Modeling the Dynamic Effects of Vegetation on Radiowave Propagation," Published in *Proc. IEEE International Conference on Communication* (*ICC*), pp. 4466 - 4471, Beijing, 19 - 23 May, 2008.

In paper E a heuristic approach was used to model the dynamic effects of vegetation using available fading measurements at 2.45, 5.25, 29 and 60 GHz, and wind speed data. The complex responses of a tree to induced wind force was studied, and used to explain different phenomena observed in measurement results. By utilizing a lowpass filter and a mass-spring system, a new simulation model for generating signal fading due to a swaying tree was developed. In the model, the oscillation of each tree component was modeled as the oscillation of a mass-spring system with the mass and spring constant of the system representing the actual mass and stiffness of the wood material. The Nakagami-Rice K-factors for different wind speeds were estimated from measurements. A good agreement was found between measured and simulated CDFs and power spectral densities (PSDs) at different wind speed conditions. Depending on the wind speed and physical characteristics of the tree, the model can be used for simulating signal fading due to a swaying tree with similar dynamical and statistical characteristics as those observed from measurement results.

Paper F

Michael Cheffena and Torbjörn Ekman, "Dynamic Model of Signal Fading due to Swaying Vegetation," Submitted to *EURASIP Journal on Wireless Communications and Networking. Special Issue on Advances in Propagation Modeling for Wireless Systems*, 2008.

In paper F a theoretical model was developed to characterize the dynamic effects of vegetation using available fading measurements at 2.45, 5.25, 29 and 60 GHz, and wind speed data. It is based on Paper E. In the model a multiple mass-spring system was used to represent a tree and a turbulent wind model was used to describe the wind dynamics. Using the wind and tree models the complex response of a tree to included wind force was mathematically described and used to model the signal fading due to swaying vegetation. The model was validated in terms of CDF, autocorrelation function (ACF), level crossing rate (LCR) and average fade duration (AFD) using measurements. Good agreement was found between the measured and simulated first and second order statistics. The model can be used for simulating signal fading due to swaying vegetation which can further be used for designing and simulating FMT.

Paper G

Michael Cheffena, Lars Erling Bråten, Terje Tjelta and Torbjörn Ekman, "Time Dynamic Channel Model for Broadband Fixed Wireless Access Systems," Published in *Proc. IST 15th Mobile & Wireless Communications Summit*, Myconos, 4 - 8 June, 2006.

In paper G a dynamic wideband channel model for BFWA which combines degradations due to multipath propagation, rain and vegetation attenuation as well as scintillation effects was developed. The objective was to specify the relationship between propagation effects and combine them in such a way to give a complete channel model suitable for designing fade mitigation and simulating capacity enhancing techniques. In the model, a time varying tapped delay line model is employed to represent the multipath propagation. The time dynamic rain attenuation is modeled using the Maseng-Bakken model [26]. The vegetation attenuation is modeled by a Nakagami-Rice distribution with K-factor decreasing with wind speed. The power spectrum of amplitude scintillation reported in [56] was used to describe the dynamics of scintillation. The short-term probability density function of scintillation was modeled by a Gaussian distribution, while the long-term distribution was modeled using the Mousley-Vilar model [70]. The influences of rain on the scintillation standard deviation and on the multipath properties of the channel were also incorporated in the combined wideband channel model.

Note that the models for the multipath propagation and vegetation effects in Paper G can be replaced by the models reported in Paper B and

Paper E/F, respectively.

7 Conclusions

A good understanding of the propagation channel at millimeter wavelength is necessary for success in designing wireless systems with a given quality-of-service (QoS) and availability. Rain attenuation varies slowly while scintillation and vegetation effects result in fast signal fading. Depending on how fast the channel changes the transmission methodology of the communication system can be adapted to increase the system throughput and guaranty the required QoS and availability. In some cases, the propagation path might be affected by combination of different propagation impairments with various speed of fading dynamics. In this case, the fade counter measure need to be optimized in terms of the various fading dynamics of the channel. For proper design of FMT, not only is knowledge on the individual dynamic effects required but also knowledge on the dependency between the propagation impairments is needed.

The work presented in this thesis deals with modeling and predicting propagation effects at millimeter wavelength channels. The collective contribution of the thesis is to add understanding on the different dynamic propagation impairments between 20 - 60 GHz with emphasis on signal fading due to rain and vegetation. As a result models for rain attenuation, multipath propagation during rain, vegetation effects, and combined propagation impairments where developed. In addition, simulations where performed to characterize the effect of multipath propagation during rain and rain attenuation on system performance. They give an insight into the kinds of system performance analysis that can be performed using the models developed in this thesis.

This work has contributed to and improved the ability to simulate propagation effects at millimeter wavelength channels. The models presented in this thesis can be used for simulating different capacity enhancing techniques such as adaptive coding and modulation and other FMT. The main contributions of this thesis and suggestions for future research are given in the following sections.

7.1 Main Contributions of the Thesis

The main contributions of the thesis can now be summarized as follows:

- A new dynamic space-time rain attenuation model was developed using available measurements at 42 GHz from a star-like network collected over four years.

- A new prediction model for fade duration statistics for satellite links between 10 - 50 GHz was developed. The most significant link and climatic parameters which governs the fade duration statistics of a particular location where identified. The new model has the best performance when compared with well known existing prediction models such as the ITU-R [5], COST 205 [6] and D-H model [7] using our fade duration database.
- Two new models for simulating signal fading due to swaying vegetation were developed using available fading measurements at 2.45, 5.25, 29 and 60 GHz, and wind speed data. A heuristic and a theoretical (which includes a tree and a turbulent wind model) approaches were used to develop the simulation models.
- A new theoretical model for generating correlated multipath taps during rain for BFWA employed in dense urban area was developed. Using the developed model the role of UT antenna on system performance was investigated. From this the importance of directive UT antennas in BFWA was indicated.
- A prediction model for parameter β_s which controls the dynamics of rain attenuation in the Maseng-Bakken model was developed. The most significant link and climatic parameters which influence the dynamics of rain attenuation where identified.
- The effect of rain on the performance of BFWA was investigated using rain attenuation statistics of three converging links. Statistical results of the channel capacity and BER in the presence of rain attenuation at different service distances in scenarios with and without intercell interference are presented.
- An initial wideband dynamic channel model which combines propagation degradations due to multipath, rain, scintillation and vegetation was developed.

7.2 Suggestions for Future Research

Below are given a list of some suggestions for future works

- Verify the theoretical multipath model during rain for BFWA employed in dense urban area reported in Paper B using wideband measurements.
- More analysis of fade duration statistics for slant paths especially for locations above 50^{o} latitude.
- As the fading is composed of effects working on different time scales (fast and slow), develop channel predictors for different speed of dynamics.

- Use knowledge on the fast and slow channel variations to develop efficient adaptive coding and modulation algorithms.
- Verify the combined wideband channel model reported in Paper G using measurements, and use it to carry out a performance analysis of BFWA subject to different combinations of propagation impairments.

References

[1] R. K. Crane, *Electromagnetic Wave Propagation Through Rain.* Wiley New York, ISBN: 0-471-61376-2, 1996.

[2] H. R. Anderson, *Fixed Broadband Wireless System Design.* Wiley New York, ISBN: 0-470-84438-8, 2003.

[3] Recommendation ITU-R P.838-3, "Specific attenuation model for rain for use in prediction methods," ITU, Geneva 2005.

[4] Recommendation ITU-R P.530-11, "Propagation data and prediction methods required for the design of terrestrial line-of-sight systems," ITU, Geneva 2005.

[5] Recommendation ITU-R P.1623-1, "Prediction method of fade dynamics on Earth-space paths," ITU, Geneva 2005.

[6] COST Project 205, "Influence of the atmosphere on radiopropagation on satellite earth paths at frequencies above 10 GHz," Report EUR EN, ISBN: 92-825-5412-0, 1985.

[7] United Sates of America, "Working document toward a revision to the fade duration prediction method in recommendation ITU-R P. 1623," Doc. 3M/36, ITU-R Study Group 3, 2003.

[8] A. Paraboni and C. Riva, "A new method for the prediction of fade duration statistics in satellite links above 10 GHz," *Int. J. Satell. Commun.*, vol. 12, no. 4, pp. 387–394, 1994.

[9] L. E. Bråten, C. Amaya, and D. Rogers, "Fade durations on Earth-space links: Dependence on path and climatic parameters," *Proc. CLIMPARA*, Budapest, 28 - 30 May 2001.

[10] United Sates of America, "Working document toward a revision of recommendation ITU-R P.1623 including a new inter-fade interval prediction method," Doc. 3M/59, ITU-R Study Group 3, 2004.

[11] E. Matricciani and M. Mauri, "Rain attenuation successive fade durations and time intervals between fades in a satellite-earth link," *Electron. Lett.*, vol. 22, no. 12, pp. 656–657, June 1986.

[12] E. Vilar and A. Burgueño, "Analysis and modeling of time intervals between rain rate exceedances in the context of fade dynamics," *IEEE Trans. Commun.*, vol. 39, no. 9, pp. 1306–1312, September 1991.

[13] L. E. Bråten, C. Amaya, and D. Rogers, "Fade and inter-fade duration at Ka-band on satellite-Earth links: Modeling and system implications," *19th AIAA Int. Commun. Satell. Sys. Conf.*, no. 140, Toulouse, 17-20 April 2001.

[14] K. I. Timothy, J. T. Ong, and E. B. L. Choo, "Fade and non-fade duration statistics for Earth-space satellite link in Ku-band," *Electron. Lett.*, vol. 36, no. 10, pp. 894–895, May 2000.

[15] D. G. Sweeney and C. W. Bostian, "Implementing adaptive power control as a 30/20-GHz fade countermeasure," *IEEE Trans. Ant. Prop.*, vol. 47, no. 1, pp. 40–46, January 1999.

[16] P. A. M. Buné, H. A. J. Herben, and J. Dijk, "Rain rate profiles obtained from the dynamic behavior of the attenuation of microwave radio signals," *Radio Sci.*, vol. 23, no. 1, pp. 13–22, 1988.

[17] E. Matricciani, "Rate of change of signal attenuation from SIRIO at 11.6 GHz," *Electron. Lett.*, vol. 17, no. 3, pp. 139–141, February 1981.

[18] M. M. J. van de Kamp, "Statistical analysis of rain fade slope," *IEEE Trans. Ant. Prop.*, vol. 51, no. 8, pp. 1750–1759, August 2003.

[19] K. I. Timothy, J. T. Ong, and E. B. L. Choo, "Descriptive fade slope statistics on INTELSAT Ku-band communication link," *Electron. Lett.*, vol. 36, no. 16, pp. 1422–1424, August 2000.

[20] B. Nelson and W. L. Stutzman, "Fade slope on 10 to 30 GHz Earth-space communiction links-measurements and modelling," *IEE Proc. Microw. Ant. Prop.*, vol. 143, no. 4, pp. 353–357, August 1996.

[21] K. Kastamonitis, B. Grémont, and M. Filip, "A study of rain fade slope," *4th COST 280 MC metting.*, Prague, Czech Republic, November 2002.

[22] E. T. Salonen and P. Heikkinen, "Fade slope analysis for low elevation angle satellite links," *COST 280/COST 272 Joint Workshop*, Noordwijk, Netherlands, May 2003.

[23] H. Fukuchi, "Correlation properties of rainfall rates in the united kingdom," *IEE Proc.*, vol. 135, no. 2, April 1988.

[24] S. Bertorelli, M. Buti, and A. Paraboni, "Seasonal variations and anisotropy properties of spatial correlation for rain attenuation obtained from radar data," *IEEE Trans. Ant. Prop.*, vol. 55, no. 2, pp. 507–510, February 2007.

[25] P. Horvath and I. Frigyes, "Efficient synchronization of an FRA system with burst traffic," IST Deliverable D19, October 2002, Available: http://www.telenor.no/fou/prosjekter/embrace.

[26] T. Maseng and P. Bakken, "A stochastic dynamic model of rain attenuation," *IEEE Trans. Commun.*, vol. 29, pp. 660–669, May 1988.

[27] B. Gremont and M. Filip, "Spatio-temporal rain attenuation model for application to fade mitigation techniques," *IEEE Trans. Ant. Prop.*, vol. 52, no. 5, pp. 1245–1256, May 2004.

[28] F. Lacoste, "Modelisation de la dynamique du canal de propagation Terre-Espace en bandes Ka et EHF," PhD thesis, Supaero, France, August 2005.

[29] S. A. Kanellopoulos, A. D. Panagopoulos, and J. D. Kanellopoulos, "Calculation of the dynamic input parameter for a stochastic model simulating rain attenuation: A novel mathematical approach," *IEEE Trans. Ant. Prop.*, vol. 55, no. 11, pp. 3257–3264, November 2007.

[30] E. Matricciani, "Physical-mathematical model of the dynamic of rain attenuation based on rain rate time series and a two-layer vertical structure of precipitation," *Radio Sci.*, vol. 31, no. 2, pp. 281–295, 1996.

[31] S. A. Callaghan, "Fractal analysis and synthesis of rain fields for radio communication systems," PhD thesis, University of Portsmouth, June 2004.

[32] B. Héder and J. Bitó, "Rain attenuation time series generation applying N-state Markov model parameterised from Hungarian measurement," *ESTEC*, Noordwijk, Netherlands, November 2005.

[33] C. Capsoni, F. Fedi, C. Magistroni, A. Paraboni, and A. Pawlina, "Data and theory for a new model of the horizontal structure of rain cells for propagation applications," *Radio Sci.*, vol. 22(3), 1987.

[34] L. Féral, H. Sauvageot, L. Castanet, and J. Lemorton, "HYCELL- A new hybrid model of the rain horizontal distribution for propagation studies," *Radio Sci.*, vol. 38, no. 3, 2003.

[35] N. C. Rogers, A. Seville, J. Richter, D. Ndzi, N. Savage, R. Caldeirinha, A. K. Shukla, M. Al-Nuaimi, K. Craig, E. Vilar, and J. Austin, "A generic model of 1-60 GHz radio propagation through vegetation - Final report," Radio Agency, UK, May 2002.

[36] M. O. Al-Nuaimi and A. M. Hammoudeh, "Measurements and predictions of attenuation and scatter of microwave signals by trees," *IEE Proc. Microw. Ant. Prop.*, vol. 141, no. 2, pp. 70–76, April 1994.

[37] I. J. Dilworth and B. L. Ebraly, "Propagation effects due to foliage and building scatter at millimeter wavelengths," *IEE Int. Conf. Ant. Prop.*, vol. 2, no. 407, pp. 51–53, Eindhoven, Netherlands, 4-7 April 1995.

[38] Recommendation ITU-R P.833-6, "Attenuation in vegetation," ITU, Geneva 2007.

[39] K. H. Craig (ed), "Propagation planning procedures for LMDS," AC215 CRABS, Deliverable D3P1b, January 1999, Available: http://www.telenor.no/fou/prosjekter/crabs.

[40] A. M. Randle, "Dynamic radio channel effects from L-band foliage scatter," PhD thesis, University of York, September 1999.

[41] A. Kajiwara, "LMDS radio channel obstructed by foliages," *Proc. IEEE ICC*, vol. 3, pp. 1583–1587, June 2000.

[42] S. Perras and L. Bouchard, "Fading characteristics of RF signals due to foliage in frequency bands from 2 to 60 GHz," *Wireless Pers. Multi. Commun.*, vol. 1, pp. 267–271, October 2002.

[43] M. H. Hashim and S. Stavrou, "Dynamic impact charcterization of vegetation movements on radiowave propagation in controlled environment," *IEEE Ant. Wireless Prop. Lett.*, vol. 2, pp. 316–318, 2003.

[44] M. H. Hashim, D. Mavrakis, and S. R. Saunders, "Measurement and analysis of temporal fading due to moving vegetation," *Proc. IEE Int. Conf. Ant. Prop. (ICAP)*, vol. 2, pp. 650–653, 31 March-3 April 2003.

[45] L. M. Correia and R. Prasad, "An overview of wireless broadband communications," *IEEE Commun. Mag.*, vol. 35, no. 1, pp. 28–33, January 1997.

[46] R. Prasad, "Overview of wireless presonal communications: Microwave perspectives," *IEEE Commun. Mag.*, vol. 35, no. 4, pp. 104–108, April 1997.

[47] C. L. Dillard, T. M. Gallagher, C. W. Bostian, and D. G. Sweeney, "28 GHz scattering by brick and limestone walls," *IEEE Int. Sym. Ant. Prop.*, vol. 3, pp. 1024–1027, 22 - 27 June 2003.

[48] P. Soma, L. Cheun, S. Sun, and M. Y. W. Chia, "Propagation measurements and modelling of LMDS radio channel in Singapore," *IEEE Trans. Veh. Techn.*, vol. 52, no. 3, pp. 595–606, May 2003.

[49] H. Xu, T. S. Rappaport, R. J. Boyle, and J. H. Schaffner, "Measurements and models for 38 GHz point-to-multipoint radiowave propagation," *IEEE J. Selec. Areas Commun.*, vol. 18, no. 3, pp. 310–321, March 2000.

[50] P. B. Papazia, G. A. Hufford, and R. J. Achatz, "Study of the local multipoint distribution service radio channel," *IEEE Trans. Broad.*, vol. 43, pp. 175–184, June 1997.

[51] D. Falconer, "Multipath measurements and modeling for fixed broadband wireless systems in a residential environment," *IEEE 802.16c-00/01*, 10 - 14 January 2000.

[52] D. Falconer, W. Zhang, and N. Moayeri, "Specific recommended channel multipah models for 802.16.1 with some implications for PHY design," *IEEE 802.16.1pc-00/21*, 24 April 2000.

[53] W. Zhang and N. Moayeri, "Recommendation on channel propagation model for local multipoint distribution service," *IEEE 802.16.1pc-00/16*, 29 February 2000.

[54] H. Vasseur and D. Vanhoenacker, "Characterization and modelling of turbulence induced scintillation on millimetre-wave line-of-sight links," *IEE Int. Conf. Ant. Prop.*, vol. 2, no. 407, pp. 292–295, Eindhoven, Netherlands, 4 - 7 April 1995.

[55] R. S. Cole, K. Ho, and N. Mavrokoukoulakis, "The effect of outer scale of turbulence and wavelength on scintillation fading at millime-

ter wavelegths," *IEEE Trans. Ant. Prop.*, vol. 26, no. 5, pp. 712–715, September 1978.

[56] A. Ishimaru, "Wave propagation and scattering in random media," *IEEE Press and Oxford University Press*, 1997.

[57] J. Haddon and E. Vilar, "Scattering induced microwave scintillations from clear air and rain on earth space paths and the influence of antenna aperture," *IEEE Trans. Ant. Prop.*, vol. 34, no. 5, pp. 646–657, May 1986.

[58] E. Matricciani, C. Riva, and M. Mauri, "Scintillation and simultaneous rain attenuation at 49.5 GHz," *Proc. Int. Conf. Ant. Prop.*, vol. 2, no. 407, pp. 165–168, Eindhoven, Netherlands, 4-7 April 1995.

[59] S. R. Saunders, *Antennas and Propagation for Wireless Communication Systems.* Wiley New York, ISBN: 0-471-98609-7, 1999.

[60] C. Catalán and E. Vilar, "Simultaneous analysis of downlink beacon dynamics and sky brightness temperature-Part II: Extraction of amplitude scintillations," *IEEE Trans. Ant. Prop.*, vol. 50, no. 4, pp. 535–544, April 2002.

[61] V. I. Tatarskii, *Wave Propagation in a Turbulent Medium.* McGraw-Hill New York, 1967.

[62] V. I. Tatarskii, "The effects of turbulent atmosphere on wave propagation," Israel program for scientific translation, Jerusalem, Israel, 1971.

[63] H. Vasseur, "Prediction of tropospheric scintillation on satellite links from radiosonde data," *IEEE Tran. Ant. Prop.*, vol. 47, no. 2, pp. 293–301, February 1995.

[64] L. E. Bråten, "Comparison of predicted scintillation with data measured from the 50 GHz Italsat beacon in Norway," *Proc. 6th Ka-band Utilization Conf.*, Cleveland, 31 May - 2 June 2000.

[65] M. Cheffena, L. E. Bråten, and T. Tjelta, "Time dynamic channel model for broadband fixed wireless access systems," *3rd Int. COST 280 Workshop*, Prague, Czech Republic, 6 - 7 June 2005.

[66] M. Cheffena, L. E. Bråten, T. Tjelta, and T. Ekman, "Time dynamic channel model for broadband fixed wireless access systems," *Proc. IST 15th Mobile & Wireless Communications Summit*, Myconos, 4 - 8 June 2006.

[67] ——, "Space-time dynamic channel model for broadband fixed wireless access," *EUCAP*, Nice, 6 - 10 November 2006.

[68] T. Tjelta and R. L. Olsen and L. Martin, "Systematic development of new multivariable techniques for predicting the distribution of multipath fading on terrestrial microwave links," *IEEE Trans. Ant. Prop.*, vol. 38, no. 10, pp. 1650–1665, October 1990.

[69] P. Rice and N. Holmberg, "Comulative time statistics of surface-point rainfall rates," *IEEE Trans. Commun.*, vol. 21, no. 10, pp. 1131–1136, October 1973.

[70] T. J. Moulsley and E. Vilar, "Experimental and theoretical statistics of microwave amplitude scintillations on satellite down-links," *IEEE Trans. Ant. Prop.*, vol. AP-30, no. 6, pp. 1099–1106, November 1982.

Part II

Included papers

Paper A

Dynamic Space-Time Rain Attenuation Model

Michael Cheffena, Lars Erling Bråten, and Torbjörn Ekman

Submitted August 2007, Revised June 2008 to
IEEE Transactions on Antennas and Propagation.

Is not included due to copyright

Paper B

Theoretical Multipath Channel Model during Rain for BFWA Employed in Dense Urban Areas

Michael Cheffena and Torbjörn Ekman

Accepted for publication in
Proc. 2nd International Conference on Signal Processing and Communication Systems, Gold Coast, 15 - 17 December, 2008.

Is not included due to copyright

Paper C

Prediction Model of Fade Duration Statistics for Satellite Links between 10 - 50 GHz

Michael Cheffena and César Amaya

Accepted for publication in
IEEE Antennas and Wireless Propagation Letters, to appear in 2008.

Is not included due to copyright

Paper D

The Effect of Rain Attenuation on the Performance of BFWA around Kjeller, Norway

Michael Cheffena

Accepted for publication in
Proc. IEEE 68th Vehicular Technology Conference (VTC), Calgary, 21 - 24 September, 2008.

Is not included due to copyright

Paper E

Modeling the Dynamic Effects of Vegetation on Radiowave Propagation

Michael Cheffena and Torbjörn Ekman

Published in
Proc. IEEE International Conference on Communication (ICC), pp. 4466 - 4471, Beijing, 19 - 23 May, 2008.

Is not included due to copyright

Paper F

Dynamic Model of Signal Fading due to Swaying Vegetation

Michael Cheffena and Torbjörn Ekman

Submitted to
EURASIP Journal on Wireless Communications and Networking. Special Issue on Advances in Propagation Modeling for Wireless Systems.

Abstract

In this contribution, we use fading measurements at 2.45, 5.25, 29 and 60 GHz, and wind speed data, to study the dynamic effects of vegetation on propagating radiowaves. By utilizing a multiple mass-spring system to represent a tree and a turbulent wind model, a new simulation model for generating signal fading due to a swaying tree was developed. The model is validated in terms of the cumulative distribution function (CDF), autocorrelation function (ACF), level crossing rate (LCR) and average fade duration (AFD) using measurements. Good agreements were found between the measured and simulated first and second order statistics of the received signals at different wind conditions. In addition, the Ricean K-factors for different wind speeds were estimated from the measurements. Generally, the new model has similar dynamical and statistical characteristics as those observed in measurement and can be used for synthesizing signal fading due to a swaying tree. The synthesized fading can be used for simulating different capacity enhancing techniques such as adaptive coding and modulation and other fade mitigation techniques.

1 Introduction

In a given environment radiowaves are subjected to different propagation degradations. Among them, vegetation moving with wind can both attenuate and give a fading effect to the propagating signal. Generally, operators cannot guarantee a clear line-of-sight (LOS) to wireless customers as vegetation in the surrounding area may grow or expand over the years and obstruct the path. Therefore, understanding the dynamic vegetation effects on propagating radiowaves is important for designing fade mitigation techniques such as adaptive coding and modulation, path diversity, and other mitigation techniques.

The attenuation depends on a range of factors; such as tree type, whether trees are in leaf or wet, frequency, and pathlength through foliage [1, 2]. For frequencies above 20 GHz, leaves and needles have dimensions large compared to the wavelength, and can significantly affect the propagation conditions. The ITU-R P. 833 [3] provides a model for predicting the mean signal attenuation though vegetation. The temporal variations of the relative phase of multipath component due to movement of the tree results in fading of the received signal, and had been reported in e.g. [4–7]. The severity of the fading depends on the rate of phase changes which further depends on the movement of the tree components. Thereby, for accurate prediction of the channel characteristics, the motion of trees under the influence of wind should be taken in to account. This requires the knowledge of wind dynamics and the complex response of a tree to induced wind force. In our previous work, a heuristic approach was used to model the dynamic effects of vegetation [7]. In this paper we develop a theoretical model based on the motion of trees under the influence of wind, and is validated in terms of first and second order statistics using available measurements.

The paper begins in Section 2 by giving a brief description of the measurement set-up for measuring signal fading after propagating through vegetation and meteorological data. Section 3 discusses the wind speed dynamics. The motion of trees and their dynamic effects to propagating radio waves, and the validation of the proposed simulation model are dealt with in Section 4. Finally, conclusions are presented in Section 5.

2 Measurement Set-Up

To characterize the influence of vegetation on radiowaves, measurements were performed for a broad range of frequencies, including 2.45, 5.25, 29

TABLE F.1: Site description [5]

Site	Pathlength	Foliage Depth	Description
Site 1	63.9 m	14.3 m	3 foliated maple trees
		7.6 m	1 foliated flowering crab tree
Site 2	110 m	25 m	Several spruce and one pine tree creating a wall

and 60 GHz, in various foliage and weather conditions [5]. A sampling rate of 500 Hz was used to collect the radio frequency (RF) signals using a spectrum analyzer, multimeter, and a computer with GPIB (General Purpose Interface Bus) interface. In addition, to understand the behavior of radiowaves propagating through vegetation under different weather conditions, meteorological measurements including wind speed and precipitation were performed. The wind speed was collected every 5 seconds, and the precipitation data every 10 seconds.

The measurements were taken in two different locations, referred to as Site 1 and Site 2. The trees at Site 1 were deciduous trees, and were considered both when the trees were in full leaf and when they were out of leaf. Site 2 was populated by several coniferous trees which made a wall of trees. Table F.1 gives general site information. A detailed description of the measurements can be found in [5]. An example of received signal at 29 GHz after propagating through dry leaved deciduous trees (Site 1) is shown in Fig. F.1, and the corresponding measured wind speed is shown in Fig. F.2. These figures indicate the existence of strong wind speed dependency for signal transmission through vegetation. For a closer look, Figs. F.3 and F.4 show examples of typical measured signals during low (1 to 3 m/s) and high wind speed ($\geq$ 4.5 m/s) conditions for leaved dry deciduous trees (Site 1) at 29 GHz, respectively. Accurate modeling of the channel is needed when design mitigation techniques for the fast and deep signal variations shown in Figs. F.1 and F.4. This requires knowledge of wind dynamics and the motion of trees under the influence of wind.

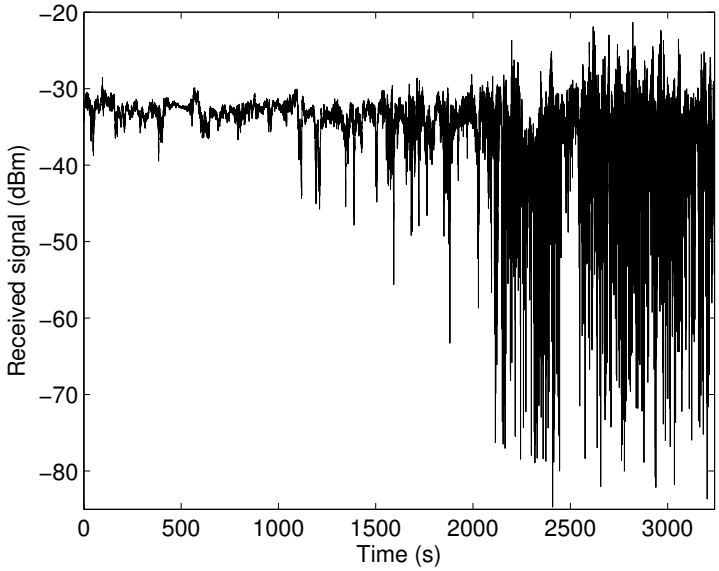

FIGURE F.1: Measured signal fading after propagating through dry leaved deciduous trees at 29 GHz.

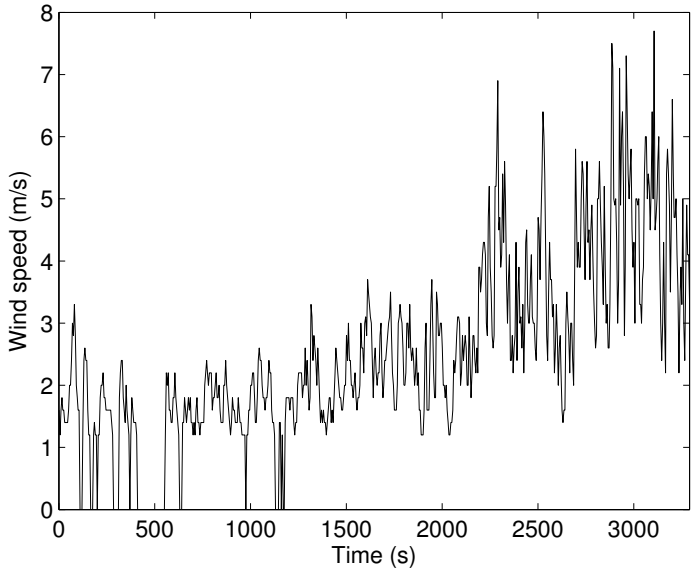

FIGURE F.2: Measured wind speed.

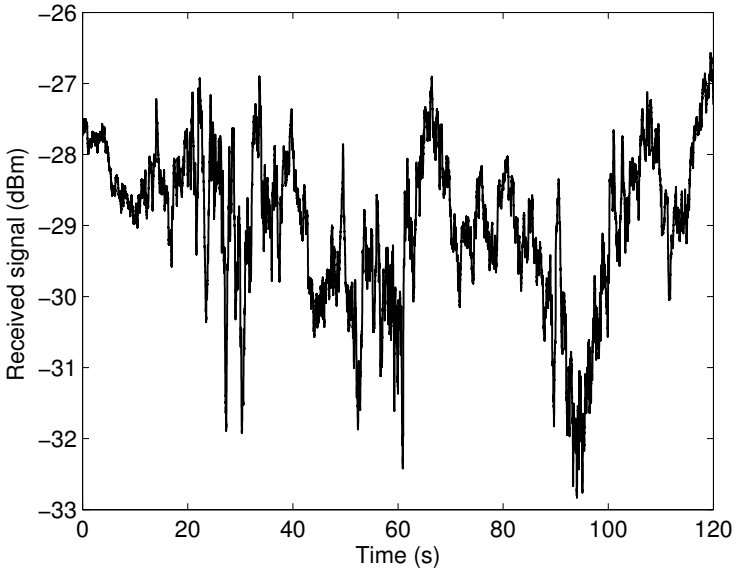

FIGURE F.3: Typical measured signal at 29 GHz for leaved dry deciduous trees during low wind speed conditions (1 to 3 m/s).

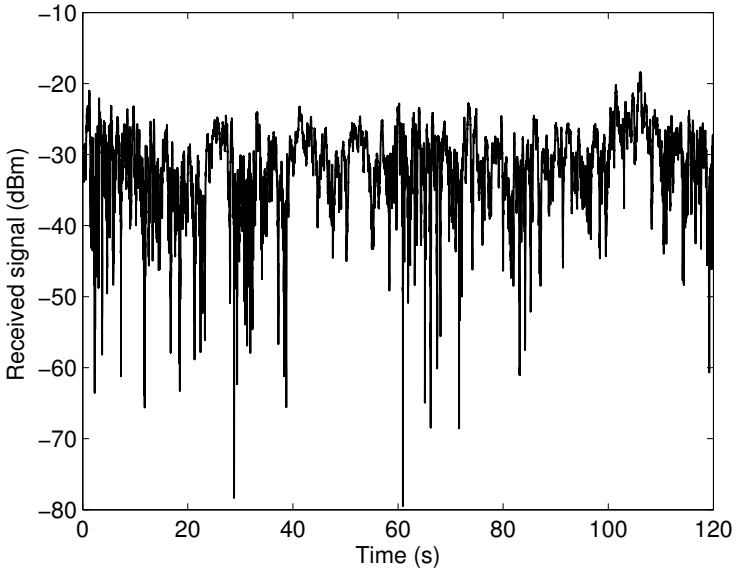

FIGURE F.4: Typical measured signal at 29 GHz for leaved dry deciduous trees during high wind speed conditions ($\geq$ 4.5 m/s).

3 Wind Dynamics

The movement of trees is directly influenced by wind. Understanding the dynamic characteristics of wind is therefore essential when describing the complex response of a tree to induced wind force and their dynamic effects to propagating radiowaves. The turbulent wind speed power spectrum can be represented by a Von Karman power spectrum [8], and it can be simulated by passing white noise through a shaping filter with transfer function given by [9, 10]

$$H_F(s) = \frac{K_F}{(1 + sT_F)^{5/6}} \tag{F.1}$$

where K_F and T_F are the gain and time constant of the shaping filter, respectively. A close approximation of the $5/6$-order filter in (F.1) by a rational transfer function is given by [9]

$$H_F(s) = K_F \frac{(g_1 T_F s + 1)}{(T_F s + 1)(g_2 T_F s + 1)} \tag{F.2}$$

where $g_1 = 0.4$ and $g_2 = 0.25$. T_f and K_F are defined as

$$T_F = \frac{L_r}{\mathrm{w}_m} \tag{F.3}$$

$$K_F \approx \sqrt{\frac{2\pi}{B(\frac{1}{2}, \frac{1}{3})} \frac{T_F}{T_s}} \tag{F.4}$$

where w_m is the mean wind speed and L_r the turbulence length scale that corresponds to the site roughness. The turbulence length can be calculated from the height, h, above the ground, expressed as $L_r = 6.5h$ [11]. T_s is the sampling period and B designates the beta function, and is given by

$$B(u, y) = \int_0^1 z^{u-1}(1 - z)^{y-1} dz \tag{F.5}$$

Fig. F.5 shows the model for simulating wind speed. In the model, a white Gaussian noise, $n(t)$ (where t is the time), with zero mean and unit variance is transformed into colored noise, $n_c(t)$ (with unite variance), by smoothing it with the filter given in (F.2). The wind speed, $\mathrm{w}(t)$, is then obtained by multiplying, $n_c(t)$, by the standard deviation of the turbulent wind, σ_w, and adding the mean wind speed, w_m, as described below.

$$\mathrm{w}(t) = n_c(t)\sigma_\mathrm{w} + \mathrm{w}_m \tag{F.6}$$

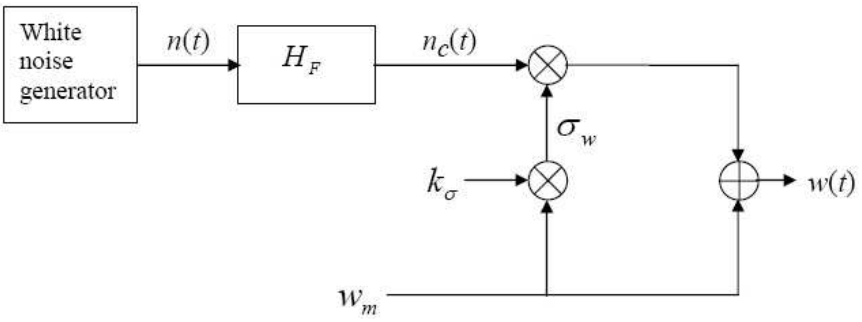

FIGURE F.5: Model for simulating wind speed.

TABLE F.2: k_σ values for different terrain types at 10 meter height [11]

Type	Coastal	Lakes	Open	Built up areas	City centres
k_σ	0.123	0.145	0.189	0.285	0.434

$$\sigma_{\mathrm{w}} = k_\sigma \mathrm{w}_m \tag{F.7}$$

where k_σ is a constant which depends on the type of the terrain [11], see Table F.2. This wind model is used in Section 4.1 to describe the displacement of tree due to induced wind force.

4 The Dynamic Effects of Vegetation on Radiowaves

4.1 The Motion of Trees

A tree is a complex structure consisting of a trunk, branches, sub-branches, and leaves. The tree responds in a complex way to induced wind forces, with each branch swaying and dynamically interacting with other branches and the trunk. During windy conditions, first-order branches sway over the swaying trunk, and second-order branches sway over the swaying first-order branches. Generally, smaller branches sway over swaying larger branches, and leaves vibrate over swaying smaller branches. The overall effect minimizes the dynamic sway of the tree by creating a broad range of frequencies and prevents the tree from failure [12]. Radiowaves scattered from these swaying tree components have a time varying phase changes due to periodic changes of the pathlength which results in fading of the received signal. Fig. F.6 illustrates the pathlength difference due to displacement of a tree component from rest, and is given by (see Appendix

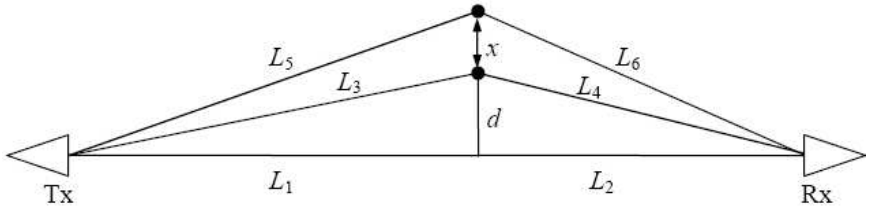

FIGURE F.6: Pathlength difference. $L_1 + L_2$ is the pathlength of the LOS component, $L_3 + L_4$ is the pathlength of the multipath component at rest, $L_5 + L_6$ is the pathlength of the multipath component when displaced, x is the displacement and d is the distance from the LOS path to the position of a tree component. Tx and Rx are the transmitting and receiving antennas.

2).

$$\Delta L \approx x\frac{d(L_1 + L_2)}{L_1 L_2} \tag{F.8}$$

where $L_1 + L_2$ is the pathlength of the LOS component. L_1 is the distance from the transmitter to a point parallel to a position of a tree component, d is the distance from L_2 to the position of a tree component, L_2 is the distance from L_1 to the receiver and x is the displacement.

A dynamic structure model of tree was reported in [12], and is extended here to include dynamic wind force and mathematical description of the motion of each tree component, see Fig. F.7. In the model, tree components (the trunk, branches and sub-branches) are attached with each other using springs which resulted in a multiple mass-spring system. This tree model is further used in Section 4.2 to model the signal fading due to swaying vegetation. For simplicity we here use a tree model with a trunk and just six branches, as seen in Fig F.7. This simple model is sufficient to recreate the rich dynamic behavior of the fading from a real tree, as is demonstrated in the simulations in Section 4.2. Using Newton's second law and the Hooke's law, the equations of motion (displacement) for the tree components in Fig. F.7 can be formulated using second order differential equations

$$\begin{aligned} m_0\ddot{x}_0(t) = &-\dot{x}_0(t)(c_0 + c_1 + c_3 + c_5) + \dot{x}_1(t)c_1 + \dot{x}_3(t)c_3 \\ &+ \dot{x}_5(t)c_5 - x_0(t)(k_0 + k_1 + k_3 + k_5) + x_1(t)k_1 \\ &+ x_3(t)k_3 + x_5(t)k_5 + f_0(t) \end{aligned} \tag{F.9}$$

$$\begin{aligned} m_1\ddot{x}_1(t) = &-\dot{x}_1(t)(c_1 + c_2) + \dot{x}_2(t)c_2 + \dot{x}_0(t)c_1 \\ &- x_1(t)(k_1 + k_2) + x_2(t)k_2 + x_0(t)k_1 + f_1(t) \end{aligned} \tag{F.10}$$

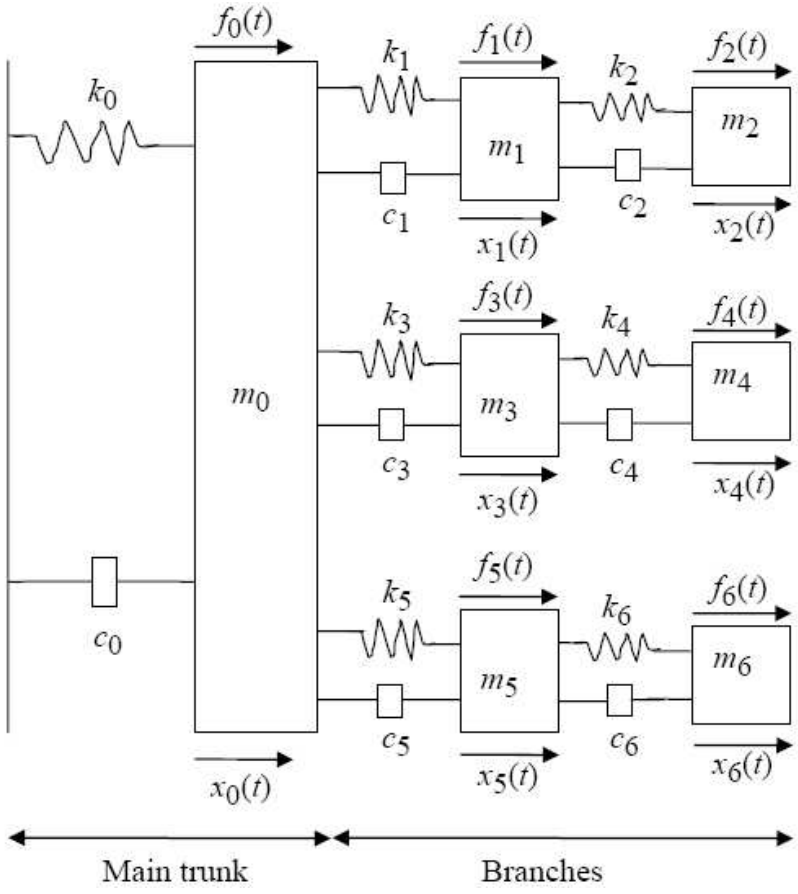

FIGURE F.7: Dynamic representation of a tree. m_i, k_i, c_i, $f_i(t)$ and $x_i(t)$ are the mass, spring constant, damping factor, time varying wind force and time varying displacement, respectively, of tree component i (the trunk and branches).

$$m_2\ddot{x}_2(t) = c_2(\dot{x}_1(t) - \dot{x}_2(t)) + k_2(x_1(t) - x_2(t)) + f_2(t) \tag{F.11}$$

$$\begin{aligned} m_3\ddot{x}_3(t) = &-\dot{x}_3(t)(c_3 + c_4) + \dot{x}_4(t)c_4 + \dot{x}_0(t)c_3 \\ &- x_3(t)(k_3 + k_4) + x_4(t)k_4 + x_0(t)k_3 + f_3(t) \end{aligned} \tag{F.12}$$

$$m_4\ddot{x}_4(t) = c_4(\dot{x}_3(t) - \dot{x}_4(t)) + k_4(x_3(t) - x_4(t)) + f_4(t) \tag{F.13}$$

$$\begin{aligned} m_5\ddot{x}_5(t) = &-\dot{x}_5(t)(c_5 + c_6) + \dot{x}_6(t)c_6 + \dot{x}_0(t)c_5 \\ &- x_5(t)(k_5 + k_6) + x_6(t)k_6 + x_0(t)k_5 + f_5(t) \end{aligned} \tag{F.14}$$

$$m_6\ddot{x}_6(t) = c_6(\dot{x}_5(t) - \dot{x}_6(t)) + k_6(x_5(t) - x_6(t)) + f_6(t) \tag{F.15}$$

where m_i, k_i and c_i are the mass, spring constant and damping factor of tree component i, respectively. The spring constant k_i describes the stiffness of the wood material. While the damping factor c_i describes the energy dissipation due to swaying tree component (aerodynamic damping) and dissipation from internal factors such as root/soil movement and internal wood energy dissipation [12]. $\ddot{x}_i(t)$, $\dot{x}_i(t)$ and $x_i(t)$ are the acceleration, velocity and position (displacement) of tree component i, respectively. $f_i(t)$ is the time varying induced wind force on tree component i, and is given by [13]

$$f_i(t) = \frac{C_d \rho \mathrm{w}(t)^2 A_i}{2} \tag{F.16}$$

where C_d is the drag coefficient, ρ is the air density, A_i is the projected surface area of the tree component and $\mathrm{w}(t)$ is the wind speed (it is assumed to be the same within the area of the tree and can be simulated using the model shown in Fig. F.5).

The time varying displacement, $x_i(t)$, of each tree component can then be obtained by solving Eqs. (F.9) to (F.15) using state-space modeling

$$\dot{\mathbf{y}} = \mathbf{A}\mathbf{y} + \mathbf{B}\mathbf{u} \tag{F.17}$$

$$\mathbf{x} = \mathbf{C}\mathbf{y} + \mathbf{D}\mathbf{u} \tag{F.18}$$

where $\mathbf{y} = [x_0(t)\ x_1(t)\ x_2(t)\ x_3(t)\ x_4(t)\ x_5(t)\ x_6(t)\ \dot{x}_0(t)\ \dot{x}_1(t)\ \dot{x}_2(t)\ \dot{x}_3(t)\ \dot{x}_4(t)\ \dot{x}_5(t)\ \dot{x}_6(t)]^T$ is the state vector, $\mathbf{u} = [f_0(t)\ f_1(t)\ f_2(t)\ f_3(t)\ f_4(t)\ f_5(t)\ f_6(t)]^T$ is the input vector, and $\mathbf{x} = [x_0(t)\ x_1(t)\ x_2(t)\ x_3(t)\ x_4(t)\ x_5(t)\ x_6(t)]^T$ is the output vector. The matrices $\mathbf{A}$, $\mathbf{B}$, $\mathbf{C}$ and $\mathbf{D}$ are obtained from Eqs. (F.9) to (F.15), see Appendix 3. Note that (F.17) and (F.18) are for continues-time and can be converted to discrete-time using e.g. bilinear transformation.

4.2 Signal Fading due to Swaying Tree

Former studies on the measurements used here suggested that the signal envelop can be represented using the Extreme value or lognormal distribution [5]. However, the majority of reported measurement results suggest Nakagami-Rice envelop distribution [6, 14–16]. It was found here that the Nakagami-Rice distribution can well represent the measured signal envelop through vegetation. The Chi-Square test has been performed to verify the fitness of Nakagami-Rice and measured signal distribution. For all frequencies, the hypothesis was accepted for 5% significance level. Therefor, Nakagami-Rice envelop distribution is assumed in the developed simulation model, with the K-factor given by

$$K = \frac{P_d}{P_f} \tag{F.19}$$

where P_d and P_f are the power in the direct and diffuse component, respectively. From our measurements we estimated the Ricean K-factors under different wind conditions using the moment-method reported in [17], see Fig. F.8. The reduction of the K-factor suggests that the contribution of the diffuse component increases with increasing wind speed. We can also observe that the K-factor decreases with increasing frequency (due to smaller wavelength).

The time series for the received power is obtain as $|h(t)^2|$ where $h(t)$ is the complex impulse response due to the multipath in the vegetation. The impulse response $h(t)$ can be expressed as

$$h(t) = a_d \exp(j\theta) + \sum_{i=0}^{6} a_f \exp\left[j\left(\theta_i - \frac{2\pi}{\lambda}\Delta L_i(t)\right)\right] \tag{F.20}$$

where $a_d = \sqrt{P_d}$ is the amplitude of the direct component and $a_f = \sqrt{P_f/7}$ is the amplitude of each scattered signal (assumed to be equal for all scattered components), θ is the phase uniformly distributed within the range [0, 2π], λ is the wavelength and $\Delta L_i(t)$ is the time varying pathlength difference due to displacement of the ith tree component shown in Fig. F.7.

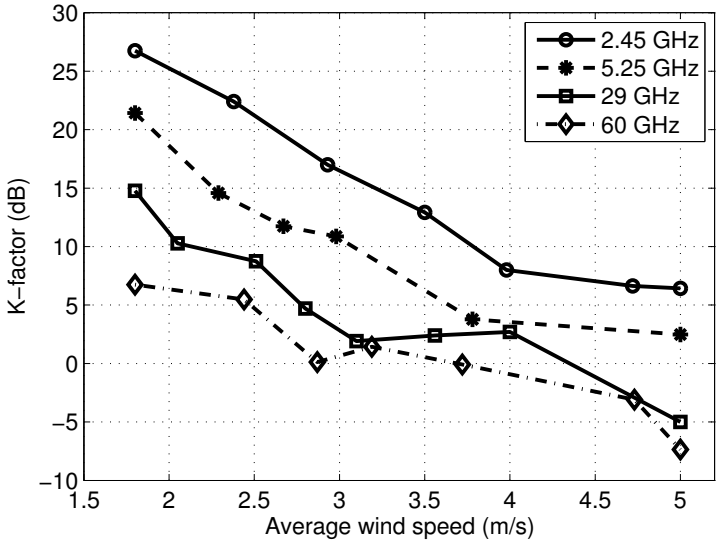

FIGURE F.8: Ricean K-factor as function of average wind speed.

Following the same approach as in (F.8), $\Delta L_i(t)$ for $i = 1, 2...6$ are given by

$$\Delta L_0(t) \approx x_0(t)\frac{d_0(L_1+L_2)}{L_1L_2} \tag{F.21}$$

$$\Delta L_1(t) \approx (x_0(t)+x_1(t))\frac{d_1(L_1+L_2)}{L_1L_2} \tag{F.22}$$

$$\Delta L_2(t) \approx (x_0(t)+x_1(t)+x_2(t))\frac{d_2(L_1+L_2)}{L_1L_2} \tag{F.23}$$

$$\Delta L_3(t) \approx (x_0(t)+x_3(t))\frac{d_3(L_1+L_2)}{L_1L_2} \tag{F.24}$$

$$\Delta L_4(t) \approx (x_0(t)+x_3(t)+x_4(t))\frac{d_4(L_1+L_2)}{L_1L_2} \tag{F.25}$$

$$\Delta L_5(t) \approx (x_0(t)+x_5(t))\frac{d_5(L_1+L_2)}{L_1L_2} \tag{F.26}$$

$$\Delta L_6(t) \approx (x_0(t)+x_5(t)+x_6(t))\frac{d_6(L_1+L_2)}{L_1L_2} \tag{F.27}$$

where L_1, L_2 and d_i are as defined in (F.8). Observe from (F.20) that the time varying pathlength difference, $\Delta L_i(t)$, results in time varying phase changes which gives a fading effect to the received signal.

Examples of simulated signal fading due to swaying tree using the new model for low and high wind speed conditions are shown in Figs. F.9 and F.10, respectively. The simulation parameters are shown in Table F.3. The parameters for the tree (A_i, m_i, k_i and c_i) are chosen to give good agreement with measurement results. Note that different damping factors, c_i, for low and high wind conditions are used. This is because as the wind speed increases tree components sway to dispute the energy induced from the wind [12] which results in increasing damping factor with increasing wind speed. In general, A_i values in the range 10 to 80 m^2, m_i values in the range 0.01 to 30 kg, k_i values in the range 5×10^2 to 5×10^4 N/m^2, c_i values in the range 0.01 to 35 (for low wind speed) and c_i values in the range 40 to 200 (for high wind speed) can be used in the model. Comparisons of the CDFs, ACFs, LCRs and AFDs of the measured (leaved dry deciduous trees (Site 1) at 29 GHz) and simulated received signals during low and high wind speed conditions are shown in Figs. F.11 - F.14. The LCRs and AFDs are normalized to the Root-Mean-Square (RMS) level. Observe that good agreement is found between the measured and simulated received signals in terms both first and second order statistics. Observe also the effects of wind speed on the first and second order statistics of the received signal. For example note how fast the ACF decays during high wind speed compared to low wind speed conditions. The increase rate of signal changing activity during windy conditions can be implied from the LCR curves in Fig. F.13. In addition, the effect of high wind speed which results in deep signal fading with short durations can be observed from the AFD curves shown in Fig. F.14.

5 Conclusion

In this paper, we use available measurements at 2.45, 5.25, 29 and 60 GHz, and wind speed data to study the dynamic effects of vegetation on propagating radiowaves. By using a multiple mass-spring system to represent a tree and a turbulent wind model to characterize the dynamic behavior of wind, a new simulation model was developed for simulating signal fading due to swaying vegetation. The model was validated in terms of first and second order statistics such as CDF, ACF, LCR and AFD at different wind conditions using measurements. Good agreements were found between the measured and simulated first and second order statistics of the received

TABLE F.3: Simulation parameters

Wind parameters		Other parameters			
$w_m = 2$ m/s (low wind)	$C_d = 0.35$ [13]	Frequency = 29 GHz			
$w_m = 5$ m/s (high wind)	$\rho = 1.226$ kg/m^3[13]	K-factor = 11 dB (at $w_m = 2$ m/s)			
$k_\sigma = 0.434$	$T_s = 0.002$ s	K-factor = -5 dB (at $w_m = 5$ m/s)			
$h = 10$ m		$L_1 = 3000$ m and $L_2 = 100$ m			
Tree parameters					
				(Low wind)	(High wind)
$d_0 = 1.0$ m	$A_0 = 78.7$ m^2	$m_0 = 20$ kg	$k_0 = 1.0 \times 10^4$ N/m	$c_0 = 32.0$	$c_0 = 189$
$d_1 = 3.0$ m	$A_1 = 33.5$ m^2	$m_1 = 1.0$ kg	$k_1 = 1.0 \times 10^3$ N/m	$c_1 = 20.0$	$c_1 = 147$
$d_2 = 3.7$ m	$A_2 = 20.3$ m^2	$m_2 = 0.02$ kg	$k_2 = 7.0 \times 10^3$ N/m	$c_2 = 0.01$	$c_2 = 43$
$d_3 = 2.5$ m	$A_3 = 35.4$ m^2	$m_3 = 2.0$ kg	$k_3 = 6.0 \times 10^2$ N/m	$c_3 = 23.0$	$c_3 = 158$
$d_4 = 2.7$ m	$A_4 = 22.2$ m^2	$m_4 = 0.03$ kg	$k_4 = 8.0 \times 10^3$ N/m	$c_4 = 0.05$	$c_4 = 42$
$d_5 = 2.8$ m	$A_5 = 36.0$ m^2	$m_5 = 2.5$ kg	$k_5 = 1.1 \times 10^3$ N/m	$c_5 = 21.0$	$c_5 = 149$
$d_6 = 3.2$ m	$A_6 = 22.9$ m^2	$m_6 = 0.04$ kg	$k_6 = 5.0 \times 10^3$ N/m	$c_6 = 0.01$	$c_6 = 44$

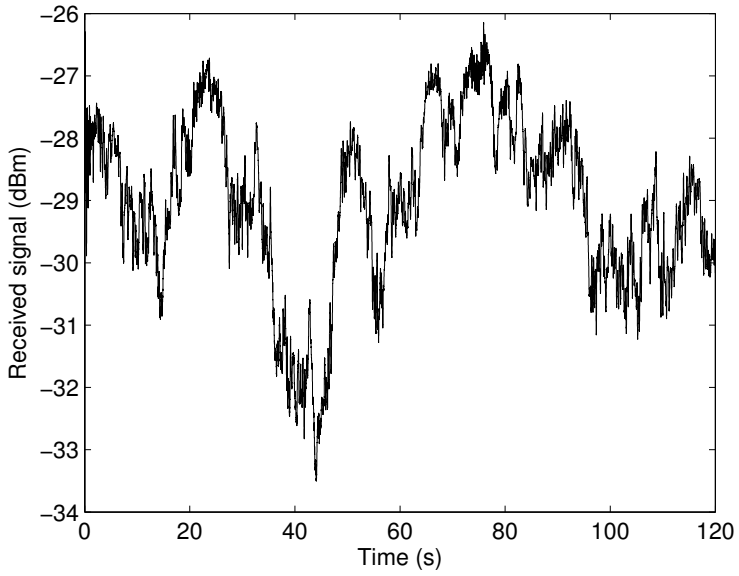

FIGURE F.9: Simulated signal fading at 29 GHz during low wind speed conditions ($w_m = 2$ m/s).

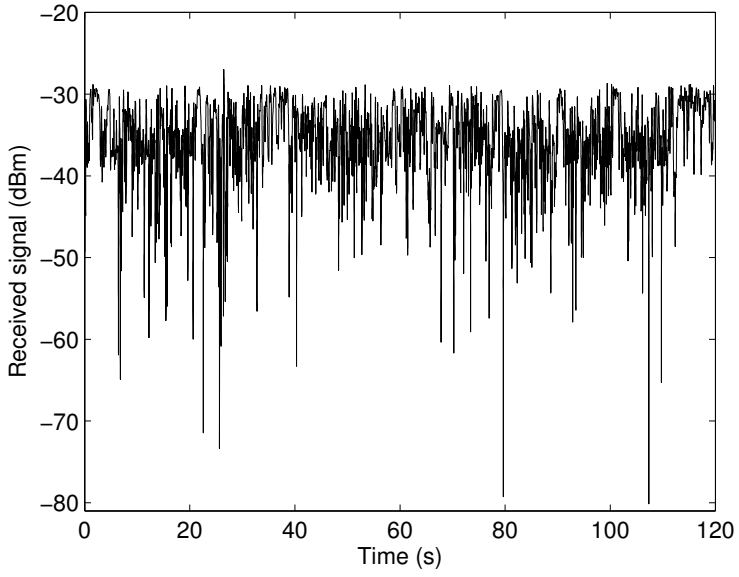

FIGURE F.10: Simulated signal fading at 29 GHz during high wind speed conditions ($w_m = 5$ m/s).

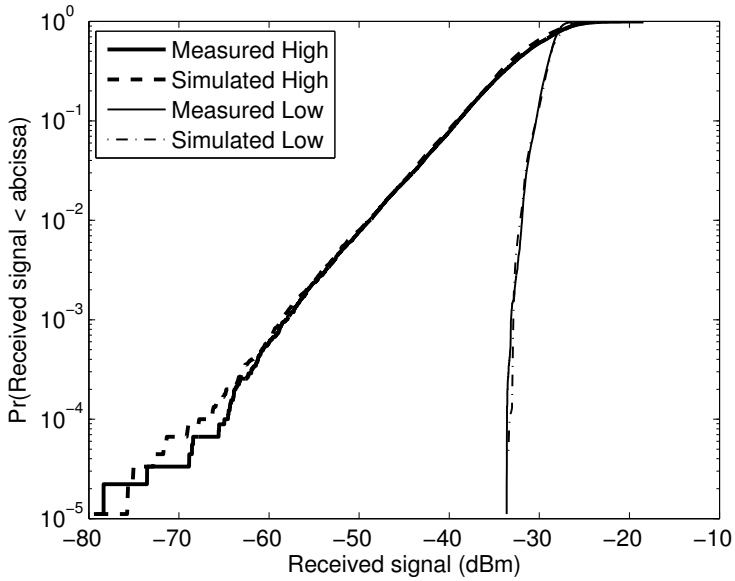

FIGURE F.11: Measured and simulated CDFs at 29 GHz for low ($w_m = 2$ m/s) and high ($w_m = 5$ m/s) wind speed conditions.

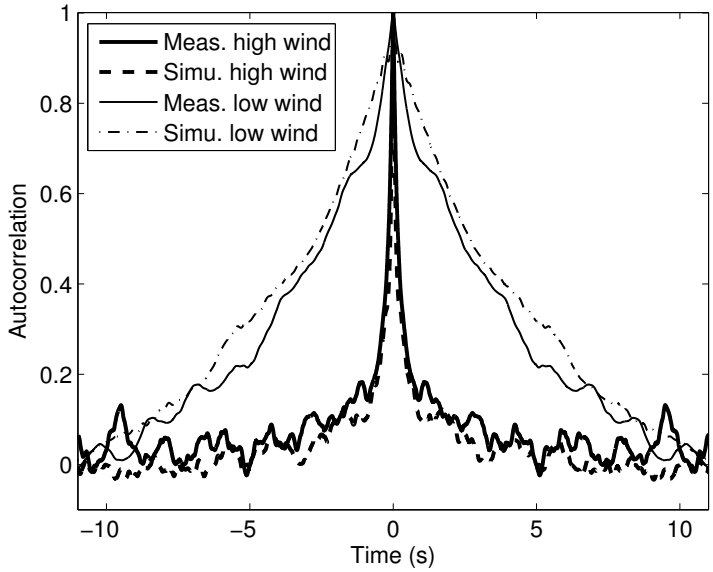

FIGURE F.12: Measured and simulated ACFs at 29 GHz for low ($w_m = 2$ m/s) and high ($w_m = 5$ m/s) wind speed conditions.

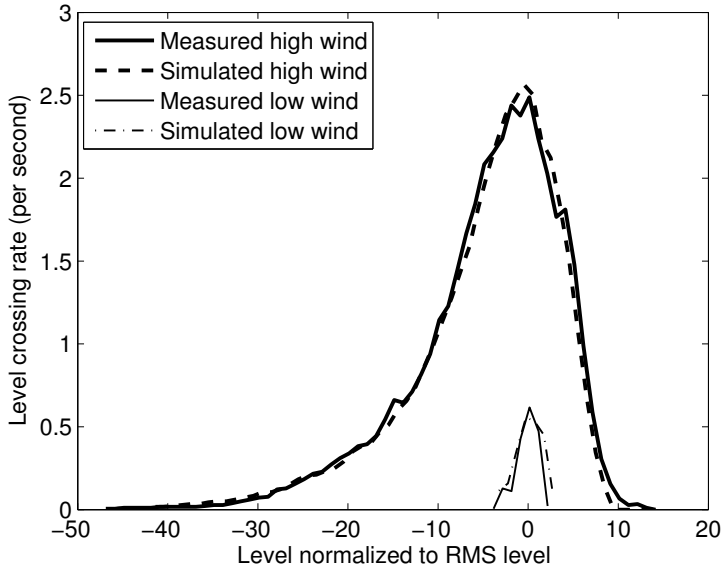

FIGURE F.13: Measured and simulated LCRs at 29 GHz for low ($w_m = 2$ m/s) and high ($w_m = 5$ m/s) wind speed conditions.

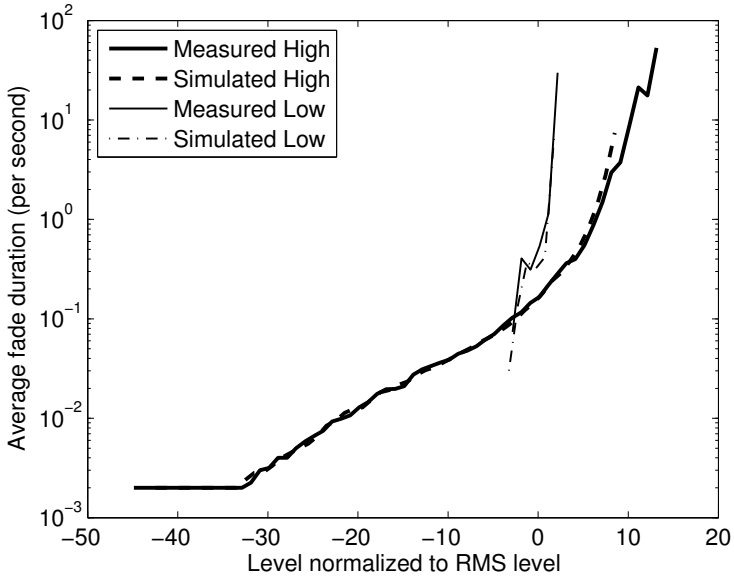

FIGURE F.14: Measured and simulated AFDs at 29 GHz for low ($w_m = 2$ m/s) and high ($w_m = 5$ m/s) wind speed conditions.

signals. Furthermore, the Ricean K-factors for different wind speeds were estimated from measurements. In general, the new model has similar dynamical and statistical characteristics as those observed from measurement results and can be used for simulating different capacity enhancing techniques such as adaptive coding and modulation and other fade mitigation techniques.

References

[1] M. O. Al-Nuaimi and A. M. Hammoudeh, "Measurements and predictions of attenuation and scatter of microwave signals by trees," *IEE Proc. Microw. Ant. Prop.*, vol. 141, no. 2, pp. 70–76, April 1994.

[2] I. J. Dilworth and B. L. Ebraly, "Propagation effects due to foliage and building scatter at millimeter wavelengths," *IEE Ant. Prop. Conf.*, vol. 2, no. 407, pp. 51–53, Eindhoven, Netherlands, 4-7 April 1995.

[3] Recommendation ITU-R P.833-5, "Attenuation in vegetation," ITU, Geneva, 2005.

[4] A. M. Randle, "Dynamic radio channel effects from L-band foliage scatter," PhD thesis, University of York, September 1999.

[5] S. Perras and L. Bouchard, "Fading characteristics of RF signals due to foliage in frequency bands from 2 to 60 GHz," *Wireless Pers. Multi. Commun.*, vol. 1, pp. 267–271, October 2002.

[6] M. H. Hashim and S. Stavrou, "Dynamic impact charcterization of vegetation movements on radiowave propagation in controlled environment," *IEEE Ant. Wireless Prop. Lett.*, vol. 2, pp. 316–318, 2003.

[7] M. Cheffena and T. Ekman, "Modeling the dynamic effects of vegetation on radiowave propagation," *Proc. IEEE ICC*, pp. 4466–4471, Beijing, China, 19 - 23 May 2008.

[8] W. E. Leithead, S. Delasalle, and D. Reardon, "Role and objectives of control for wind turbines," *IEE Proc. Gener. Transm. Distrib.*, vol. 138, no. 2, pp. 135–148, 1991.

[9] C. Nichita, D. Luca, B. Dakyo, and E. Ceanga, "Large band simulation of the wind speed for real time wind turbine simulators," *IEEE Trans. Energy Convers.*, vol. 17, no. 4, pp. 523–529, December 2002.

[10] E. B. Muhando, T. Senjyu, N. Urasaki, A. Yona, H. Kinjo, and T. Funabashi, "Gain scheduling control of variable speed WTG under widely varying turbulence loading," Renewable Energy (In Press), 2007.

[11] *European Standard for Wind Loads*, Eurocode EN 1991-1-4, WIND ACTION.

[12] K. R. James, N. Haritos, and P. K. Ades, "Mechanical stability of trees under dynamic loads," *American Journal of Botany*, vol. 93, no. 10, pp. 1522–1530, 2006.

[13] H. Peltola, S. Kellomäki, H. Väisänen, and V. P. Ikonen, "A mechanistic model for assessing the risk of wind and snow damage to single trees and stands of Scots pine, Norway spruce, and birch," *Can. J. For. Res.*, vol. 29, pp. 647–661, 1999.

[14] J. C. DalBello, G. L. Siqueira, and H. L. Bertoni, "Effects of vegetation on urban cellular systems," *Proc. IEEE Univ. Pers. Commun. Conf., ICUPC*, vol. 1, pp. 113–116, October 1998.

[15] A. Kajiwara, "LMDS radio channel obstructed by foliages," *Proc. IEEE ICC*, vol. 3, pp. 1583–1587, June 2000.

[16] N. Naz and D. D. Falconer, "Temporal variations characterization for fixed wireless at 29.5 GHz," *Proc. IEEE Veh. Tech. Conf.*, vol. 3, pp. 2178–2182, May 2000.

[17] L. J. Greenstein, D. G. Michelson, and V. Erceg, "Moment-method estimation of the Ricean K-factor," *IEEE Commun. Lett.*, vol. 3, no. 6, pp. 175–176, 1999.

Paper G

Time Dynamic Channel Model for Broadband Fixed Wireless Access Systems

Michael Cheffena, Lars Erling Bråten, Terje Tjelta and Torbjörn Ekman

Published in
Proc. IST 15th Mobile & Wireless Communications Summit, Myconos, 4 - 8 June, 2006.

Is not included due to copyright

Abstract

Broadband fixed wireless access (BFWA) has been recognized as an effective first kilometer solution for delivering broadband services to residential and business customers. The large bandwidths available above 20 GHz make radio systems with very high capacities possible. Users can be offered bit rates in the order of several hundred Mbit/s. Such radio links can, in many cases, be an alternative to optical fibre in terms of capacity. This article presents a time dynamic channel model for BFWA operating above 20 GHz. The developed channel model represents the time varying wideband channel, and combines degradations due to multipath propagation, rain and vegetation attenuation as well as scintillation effects. A time varying tapped delay line model is employed to represent multipath propagation. Time dynamic rain attenuation is modeled using the Maseng-Bakken model. The vegetation attenuation is modeled by a Nakagami-Rice distribution with K-factor decreasing with wind speed. The short-term probability density function of amplitude scintillation is modeled by a Gaussian distribution, while the long-term distribution is modeled using the Mousley-Vilar model. The combined channel model is suitable for simulating fading mitigation techniques such as adaptive coding and modulation, interference cancellation, and other capacity enhancing techniques.

Part III

Appendices

Appendix 1

Derivation of (A.11)

The correlation coefficient between two filter outputs is given by

$$[R_Y]_{ij} = E[y_i(k)y_j(k)] \tag{1.1}$$

where $y_i(k)$ and $y_j(k)$ are given by (A.10); substituting these expressions in (1.1) yields

$$\begin{aligned}
[R_Y]_{ij} &= E[(\sqrt{1-\rho_i^2}x_i(k) + \rho_i y_i(k-1)) \cdot (\sqrt{1-\rho_j^2}x_j(k) + \rho_j y_j(k-1)] \\
&= \sqrt{1-\rho_i^2}\sqrt{1-\rho_j^2}\overbrace{E[x_i(k)x_j(k)]}^{[R_X]_{ij}} + \rho_j\sqrt{1-\rho_i^2}\overbrace{E[x_i(k)y_j(k-1)]}^{0} \\
&\quad + \rho_i\sqrt{1-\rho_j^2}\overbrace{E[x_j(k)y_i(k-1)]}^{0} + \rho_i\rho_j\overbrace{E[y_i(k-1)y_j(k-1)]}^{[R_Y]_{ij}} \\
&= \sqrt{1-\rho_i^2}\sqrt{1-\rho_j^2}[R_X]_{ij} + \rho_i\rho_j[R_Y]_{ij}
\end{aligned} \tag{1.2}$$

Solving (1.2) for $[R_X]_{ij}$ gives

$$[R_X]_{ij} = \frac{1-\rho_i\rho_j}{\sqrt{1-\rho_i^2}\sqrt{1-\rho_j^2}}\,[R_Y]_{ij} \tag{1.3}$$

Appendix 2

Derivation of (F.8)

From Fig. F.6, by using Pythagoras

$$\begin{aligned} L_3 &= \sqrt{L_1^2 + d^2} \\ &= L_1\sqrt{1 + \frac{d^2}{L_1}} \end{aligned} \tag{2.1}$$

Applying Taylor approximation

$$L_3 \approx L_1(1 + \frac{d^2}{2L_1^2}) \tag{2.2}$$

Similarly

$$L_4 \approx L_2(1 + \frac{d^2}{2L_2^2}) \tag{2.3}$$

$L_3 + L_4$ is the pathlength in rest, and is given by

$$L_3 + L_4 = L_1 + L_2 + \frac{d^2}{2}\left(\frac{L_1 + L_2}{L_1 L_2}\right) \tag{2.4}$$

$L_5 + L_6$ is the pathlength when displaced, expressed as

$$L_5 + L_6 = L_1 + L_2 + \frac{(d+x)^2}{2}\left(\frac{L_1 + L_2}{L_1 L_2}\right) \tag{2.5}$$

The difference in pathlength when a branch is in rest and when it is displaced is then given by

$$\begin{aligned} \Delta L &= L_5 + L_6 - L_3 + L_4 \\ &= \frac{(2dx + x^2)}{2} \left(\frac{L_1 + L_2}{L_1 L_2} \right) \\ &\approx x \frac{d(L_1 + L_2)}{L_1 L_2} \end{aligned} \tag{2.6}$$

Appendix 3

Matrices for the State-Space Model in (F.17) and (F.18)

$$\mathbf{A} = \begin{pmatrix} \mathbf{0_{7\times 7}} & \mathbf{I_{7\times 7}} \\ \mathbf{A_{21}} & \mathbf{A_{22}} \end{pmatrix} \tag{3.1}$$

where $\mathbf{0_{7\times 7}}$ and $\mathbf{I_{7\times 7}}$ are 7 by 7 zero and identity matrices, respectively. $\mathbf{A_{21}}$ and $\mathbf{A_{22}}$ are given by

$$\mathbf{A_{21}} = \begin{pmatrix} -\frac{(k_0+k_1+k_3+k_5)}{m_0} & \frac{k_1}{m_0} & 0 & \frac{k_3}{m_0} & 0 & \frac{k_5}{m_0} & 0 \\ \frac{k_1}{m_1} & -\frac{(k_1+k_2)}{m_1} & \frac{k_2}{m_1} & 0 & 0 & 0 & 0 \\ 0 & \frac{k_2}{m_2} & -\frac{k_2}{m_2} & 0 & 0 & 0 & 0 \\ \frac{k_3}{m_3} & 0 & 0 & -\frac{(k_3+k_4)}{m_3} & \frac{k_4}{m_3} & 0 & 0 \\ 0 & 0 & 0 & \frac{k_4}{m_4} & -\frac{k_4}{m_4} & 0 & 0 \\ \frac{k_5}{m_5} & 0 & 0 & 0 & 0 & -\frac{(k_5+k_6)}{m_5} & \frac{k_6}{m_5} \\ 0 & 0 & 0 & 0 & 0 & \frac{k_6}{m_6} & -\frac{k_6}{m_6} \end{pmatrix} \tag{3.2}$$

$$\mathbf{A_{22}} = \begin{pmatrix} -\frac{(c_0+c_1+c_3+c_5)}{m_0} & \frac{c_1}{m_0} & 0 & \frac{c_3}{m_0} & 0 & \frac{c_5}{m_0} & 0 \\ \frac{c_1}{m_1} & -\frac{(c_1+c_2)}{m_1} & \frac{c_2}{m_1} & 0 & 0 & 0 & 0 \\ 0 & \frac{c_2}{m_2} & -\frac{c_2}{m_2} & 0 & 0 & 0 & 0 \\ \frac{c_3}{m_3} & 0 & 0 & -\frac{(c_3+c_4)}{m_3} & \frac{c_4}{m_3} & 0 & 0 \\ 0 & 0 & 0 & \frac{c_4}{m_4} & -\frac{c_4}{m_4} & 0 & 0 \\ \frac{c_5}{m_5} & 0 & 0 & 0 & 0 & -\frac{(c_5+c_6)}{m_5} & \frac{c_6}{m_5} \\ 0 & 0 & 0 & 0 & 0 & \frac{c_6}{m_6} & -\frac{c_6}{m_6} \end{pmatrix} \tag{3.3}$$

$$\mathbf{B} = \begin{pmatrix} 0 & 0 & 0 & 0 & 0 & 0 & 0 \\ 0 & 0 & 0 & 0 & 0 & 0 & 0 \\ 0 & 0 & 0 & 0 & 0 & 0 & 0 \\ 0 & 0 & 0 & 0 & 0 & 0 & 0 \\ 0 & 0 & 0 & 0 & 0 & 0 & 0 \\ 0 & 0 & 0 & 0 & 0 & 0 & 0 \\ 0 & 0 & 0 & 0 & 0 & 0 & 0 \\ \frac{1}{m_0} & 0 & 0 & 0 & 0 & 0 & 0 \\ 0 & \frac{1}{m_1} & 0 & 0 & 0 & 0 & 0 \\ 0 & 0 & \frac{1}{m_2} & 0 & 0 & 0 & 0 \\ 0 & 0 & 0 & \frac{1}{m_3} & 0 & 0 & 0 \\ 0 & 0 & 0 & 0 & \frac{1}{m_4} & 0 & 0 \\ 0 & 0 & 0 & 0 & 0 & \frac{1}{m_5} & 0 \\ 0 & 0 & 0 & 0 & 0 & 0 & \frac{1}{m_6} \end{pmatrix} \tag{3.4}$$

$$\mathbf{C} = \begin{pmatrix} 1 & 0 & 0 & 0 & 0 & 0 & 0 & 0 & 0 & 0 & 0 & 0 & 0 & 0 \\ 0 & 1 & 0 & 0 & 0 & 0 & 0 & 0 & 0 & 0 & 0 & 0 & 0 & 0 \\ 0 & 0 & 1 & 0 & 0 & 0 & 0 & 0 & 0 & 0 & 0 & 0 & 0 & 0 \\ 0 & 0 & 0 & 1 & 0 & 0 & 0 & 0 & 0 & 0 & 0 & 0 & 0 & 0 \\ 0 & 0 & 0 & 0 & 1 & 0 & 0 & 0 & 0 & 0 & 0 & 0 & 0 & 0 \\ 0 & 0 & 0 & 0 & 0 & 1 & 0 & 0 & 0 & 0 & 0 & 0 & 0 & 0 \\ 0 & 0 & 0 & 0 & 0 & 0 & 1 & 0 & 0 & 0 & 0 & 0 & 0 & 0 \end{pmatrix} \tag{3.5}$$

$$\mathbf{D} = (\mathbf{0_{7\times 7}}) \tag{3.6}$$